Am J Cancer Res 2022;12(11):5183-5204
www.ajcr.us /ISSN:2156-6976/ajcr0144008

Original Article

MECP2 promotes the migration and invasion of gastric cancer cells by modulating the Notch1/c-Myc/mTOR signaling pathways by suppressing FBXW7 transcription

Lingyu Zhao[1,2], Xiaofei Wang[1], Juan Yang[1,2], Qiuyu Jiang[1,2], Jing Zhang[3], Feng Wu[4], Lei Ni[1], Dongdong Tong[1,2], Chen Huang[1,2]

[1]Department of Cell Biology and Genetics/Key Laboratory of Environment and Genes Related to Diseases, School of Basic Medical Sciences, Xi'an Jiaotong University Health Science Center, Xi'an 710061, Shaanxi, China; [2]Institute of Genetics and Developmental Biology, Translational Medicine Institute, School of Basic Medical Sciences, Xi'an Jiaotong University Health Science Center, Xi'an 710061, Shaanxi, China; [3]Department of Clinical Medicine, Medical College of Yan'an University, Yan'an 716000, Shaanxi, China; [4]Center of Teaching and Experiment for Medical Post Graduates, Xi'an Jiaotong University Health Science Center, Xi'an 710061, Shaanxi, China

Received May 8, 2022; Accepted October 14, 2022; Epub November 15, 2022; Published November 30, 2022

Abstract: Methyl-CpG-binding protein 2 (MECP2), an epigenetic regulatory factor, promotes the carcinogenesis and progression of a number of cancers. However, its role in the migration and invasion of gastric cancer (GC), as well as the underlying molecular mechanisms, remain unclear. In this study, we found that MECP2 promoted the migration, invasion and metastasis of GC cells. Investigation of the molecular mechanism revealed that MECP2 repressed F-box and WD40 domain protein 7 (FBXW7) transcription in GC by binding to the methylated CpG sites in the FBXW7 promoter region. MECP2 expression was markedly negatively correlated with the FBXW7 level in GC tissues. FBXW7 expression was significantly downregulated in GC tissues and cell lines, and low FBXW7 expression was correlated with unfavorable clinicopathologic features. FBXW7 inhibited cell migration and invasion by regulating the Notch1/c-Myc/mTOR signaling pathways, and knockdown of FBXW7 reversed the effects of silencing MECP2. Moreover, MECP2 upregulated the Notch1/c-Myc/mTOR signaling pathways by inhibiting FBXW7 expression at the transcriptional level. This study demonstrates that MECP2 promotes the migration and invasion of GC cells by modulating the Notch1/c-Myc/mTOR signaling pathways via suppression of FBXW7 transcription. These findings suggest that MECP2 may be a novel effective therapeutic target in GC.

Keywords: MECP2, gastric cancer, FBXW7, migration, invasion, Notch1 signaling pathway

Introduction

Gastric cancer (GC) remains the fifth most common malignancy and the third most frequent cause of cancer-related deaths worldwide, and its morbidity and mortality are highest in East Asia [1, 2]. Although the incidence of GC has decreased appreciably in the last few decades, approximately 679,000 new GC cases are diagnosed and 498,000 GC cancer-associated deaths occur China every year [3]. At present, GC patients are usually treated with a combination of surgery, chemotherapy and radiotherapy, but the effect is unsatisfactory because GC is a highly complex disease. In particular, the molecular mechanisms of GC metastasis and invasion, which are responsible for nearly 90% of deaths among GC patients, are still not fully understood [4-6]. Therefore, it is crucial to investigate genes that govern GC metastasis and invasion to elucidate the molecular mechanisms and develop more effective therapeutic strategies.

Methyl-CpG-binding protein 2 (MECP2), belonging to the methyl-CpG-binding domain (MBD) family, contains an MBD and a transcriptional repression domain (TRD) [7-9]. An important epigenetic regulatory factor, MECP2 modulates chromatin organization and gene transcription by binding to the methylated DNA sites in the promoter regions of genes [10, 11]. It is an

X-linked gene whose mutation results in neurological disorders, such as Rett syndrome [12]. It has been reported that MECP2 not only suppresses gene transcription-for example, inhibiting BDNF and Cdkl5 expression-by binding to methylated CpG islands and recruiting corepressors (e.g., histone deacetylases and Sin3A) but also promotes gene transcription-for example, promoting GIT1 expression-by binding to methylated CpG dinucleotides and recruiting activators (e.g., CREB1) [13-17]. In recent years, emerging evidence has indicated the role of MECP2 as a crucial oncogene in several cancer types [18]. Our previous studies found that MECP2 is upregulated in liver cancer and facilitates cell growth [19], enhances breast cancer cell proliferation by facilitating ubiquitination-mediated P53 degradation via regulation of RPL5/RPL11 expression [20], and promotes the proliferation and suppresses the apoptosis of GC cells by repressing FOXF1/MYOD1 transcription and enhancing GIT1 transcription by binding to the methylated CpG sites in the promoter regions of FOXF1/MYOD1 [21, 22]. Cancer cell migration and invasion are related to the metastatic potential of the cells, which may be independent of the proliferation rate. To date, the function of MECP2 in cancer cell migration and invasion has not been precisely studied. In particular, the role of MECP2 in the migration and invasion of GC cells remains unknown.

To address the abovementioned knowledge gap, we investigated the effect of MECP2 on GC cell migration and invasion and explored the underlying molecular mechanism. The results demonstrated that MECP2 promoted the migration and invasion of GC cells. Chromatin immunoprecipitation sequencing (ChIP-Seq) and the luciferase reporter assay showed that MECP2 inhibited F-box and WD40 domain protein 7 (FBXW7) transcription by binding to the methylated CpG sites in the FBXW7 promoter region. Western blot and qRT-PCR analyses revealed lower expression of FBXW7 in GC tissues, which was correlated with unfavorable clinicopathological features. MECP2 expression was negatively correlated with FBXW7 expression. FBXW7 inhibited the migration and invasion of GC cells. Further molecular mechanistic investigations showed that MECP2 promoted cell migration and invasion by regulating the Notch1/c-Myc/mTOR signaling pathways via inhibition of FBXW7 transcription. In brief, the findings in this study indicate that MECP2 may be a novel effective therapeutic target in GC.

Materials and methods

Patients and specimens

Tumor specimens and adjacent nontumor tissues were collected from 166 GC patients treated between 2015 and 2018 in the Department of Oncology Surgery, the First Affiliated Hospital of the Medical College of Xi'an Jiaotong University, China. All patients underwent curative surgical resection without radiotherapy or chemotherapy prior to surgery. Clinicopathological data of the patients were obtained from their pathology records. The study was approved by the Ethics Committee of the university. Informed consent was obtained from all patients before tissue sample collection.

Cell culture

A normal human gastric epithelial cell line (GES-1) and the human GC cell lines BGC-823 and MKN-45 were purchased from the Cell Bank (Shanghai Genechem Co., Ltd., Shanghai, China). The cell lines had been tested and authenticated by the Cell Bank. Cells were cultured in RPMI-1640 medium (Gibco BRL, Grand Island, NY, USA) containing 10% fetal bovine serum (FBS) (Gibco, USA) at 37°C in 5% CO_2 and 100% humidity. All cells were examined and confirmed to be negative for mycoplasma contamination. Cell morphology and behavior were confirmed to be consistent with the Cell Bank descriptions.

RNA extraction and quantitative real-time PCR (qRT-PCR)

Total RNA was isolated from GC tissues and cell lines using TRIzol Reagent (Invitrogen, Carlsbad, CA, USA) according to the manufacturer's protocol. Reverse transcription was performed using a commercial kit (Takara, Dalian, China). QRT-PCR was performed with a SYBR Green PCR Kit (Takara Biotechnology, Takara, Dalian, China) using an IQ5 Multicolor qRT-PCR Detection System (Bio-Rad, USA). In all qRT-PCR analyses, each specimen was analyzed in triplicate. The primer sequences are listed in Supplementary Table 1. The mRNA expression

of target genes was normalized to β-actin, and the $2^{-\Delta\Delta Ct}$ method was used to calculate expression levels.

Immunohistochemical (IHC) staining

IHC staining was performed on the tissue specimens collected from GC patients. The tissue samples were fixed with 4% paraformaldehyde, embedded in paraffin and sectioned at a thickness of 4 μm. After deparaffinization and hydration through a graded alcohol series, antigen retrieval and blocking were performed. The sections were then incubated first with the corresponding primary antibody (anti-FBXW7, Santa Cruz, CA, USA) at a dilution of 1:100 and then with a biotinylated secondary antibody (Santa Cruz, CA, USA). Subsequently, the sections were visualized using a 3,3'-diaminobenzidine (DAB) kit, counterstained with hematoxylin, and scored independently by two pathologists blinded to the patient outcomes. FBXW7 protein expression was assessed semiquantitatively. High expression was defined as a percentage of positive cells > 25% in 5 random fields; otherwise, expression was considered low. The integrated optical density (ISO) in 5 randomly selected fields was quantified using ImageJ v1.8.0 (Wayne Rasband, USA).

Plasmid construction and transfection

The full-length complementary DNA sequences of human MECP2 and FBXW7 were inserted separately into the pCMV2-GV146 vector following the manufacturer's instructions (Genechem Co., Ltd., China). Then, the wild-type and mutant plasmids, namely, pCMV2-GV146-GFP-MECP2 (WT), pCMV2-GV146-GFP-Mutation type 1 (MT1), and pCMV2-GV146-GFP-Mutation type 2 (MT2), were constructed (Supplementary Table 2). A 463-bp fragment spanning positions 153454019 to 153454481 relative to the transcription start site (TSS) of the FBXW7 promoter was inserted upstream of the firefly luciferase reporter gene (pGL3-FBXW7-luc) in the reporter plasmid pGL3-FBXW7 (Genechem Co. Ltd., Shanghai, China). The entire promoter sequence of FBXW7 was not inserted to facilitate FBXW7 transcription because other transcription factors might bind to it and affect the analysis of the results. BGC-823 and MKN-45 cells were cultured in RPMI-1640 medium without antibiotics for 24 h. Next, the pCMV2-GV146 vector, pCMV2-GV146-MECP2 plasmid or pCMV2-GV146-FBXW7 plasmid was transiently transfected into cells using Lipofectamine TM-2000 reagent (Invitrogen, Carlsbad, CA, USA). Cell assays were performed 48 h after transfection.

SiRNA synthesis and transfection

The sequences of the MECP2 siRNAs (si-MECP2-1 and si-MECP2-2) and FBXW7 siRNAs (si-FBXW7-1 and si-FBXW7-2) were predesigned and synthesized by GenePharma (SGC, Shanghai, China). A scrambled siRNA sequence was used as a negative control (NC-siRNA). All the siRNA sequences are listed in Supplementary Table 3. GC cells (BGC-823 and MKN-45) were cultured for 24 h and transfected with the indicated targeting siRNAs or NC-siRNA using Lipofectamine TM-2000 reagent in accordance with the manufacturer's instructions.

Immunofluorescence (IF)

BGC-823 and MKN-45 cells were plated on polylysine-coated coverslips in 24-well plates for 24 h and then transfected with the pCMV2-GV146-GFP plasmid or pCMV2-GV146-GFP-MECP2 plasmid for 48 h. Then, the cells were fixed with 4% paraformaldehyde at room temperature for 10 min, washed with PBS, and blocked with 10% normal goat serum in PBS containing 0.3% Triton X-100 for 1 h at room temperature. Subsequently, the cells were incubated at 4°C with an anti-GFP or anti-MECP2 primary antibody (Supplementary Table 4) overnight. Negative controls incubated without the primary antibodies were used to exclude the effects of nonspecific staining. Subsequently, the matched secondary antibodies IgG-FITC and IgG-PE were added and incubated for 2 h at 37°C, after which 4,6-diamidino-2-phenylindole (DAPI) was used to stain nuclei for 5 min. The immunostained cells were observed by indirect fluorescence under a fluorescence microscope (Olympus BX51; Olympus, Tokyo, Japan) equipped with DPManager (DPController) software (Olympus). Each experiment was conducted independently three times.

Wound healing assay

A scratch wound healing assay was performed to determine the migration capacity of human GC cells. Differently treated BGC-823 and MKN-45 cells were seeded in 6-well plates and

grown to approximately 60% confluence. A single wound was made by gently and slowly scratching with a 10 μl disposable pipette tip across the center of a well. Suspended cells were removed by washing with PBS, and the remaining cells were incubated in fresh medium. Wound closure was observed at 0 and 48 h under a microscope (Olympus, Japan). The gap width was quantitatively evaluated using ImageJ v1.8.0 (Wayne Rasband, USA). The cell migration rate was quantified by setting the average migration distance in the control group as 100%. Results were obtained from three independent experiments.

Transwell migration and invasion assays

Transwell assays were performed on BGC-823 and MKN-45 cells. To examine cell migration, differently treated cells were plated in the upper chambers of a 24-well Transwell plate (8 μm pore size; Millipore, Billerica, MA, USA) at a density of 2.0×10^4 cells in 100 μl of serum-free medium, and 600 μl of medium containing 10% serum was added to the lower chambers. The cells were then incubated for 24 h at 37°C in a 5% CO_2 atmosphere and then removed from the upper surface of each filter membrane by scraping with a cotton swab. The migrated cells adhering to the bottom surface of each membrane were fixed with 4% paraformaldehyde and stained with 0.1% crystal violet. To examine cell invasion, 4.0×10^4 cells were incubated in a chamber with a Matrigel (15 μg/filter membrane; BD Biosciences, Franklin Lakes, NJ, USA)-coated membrane for 48 h. The cells that migrated and invaded to the lower surface of the filter membrane were quantified with ImageJ v1.8.0 (Wayne Rasband, USA) in 5 random fields. The relative migration and invasion rates were measured by setting the number of cells in the control groups as 1. Each experiment was repeated three times.

Chromatin immunoprecipitation (ChIP), ChIP-Seq and ChIP-RT-PCR

Different plasmids, including the pCMV2-GV146-GFP-MECP2 (WT), pCMV2-GV146-GFP-Mutation type 1 (MT1), pCMV2-GV146-GFP-Mutation type 2 (MT2) plasmids and the empty vector, were transfected into BGC-823 cells. ChIP was performed as previously described [23]. Cultured BGC-823 cells were crosslinked with 1% formaldehyde for 15 min, and 125 mM glycine was added for quenching. A cell cracker was used to sonicate cells to obtain nuclear lysates. Chromatin was sonicated into fragments of approximate 200 bp. The collected lysates were divided into two portions. One portion was used as input, and the other was incubated with 5 μg of an anti-GFP antibody, an anti-MeCP2 antibody, or IgG (Supplementary Table 4) overnight at 4°C. Next, DNA-protein complexes were captured with Dynabeads Protein A (Invitrogen, Carlsbad, CA, USA) and eluted with TE buffer at 65°C. Crosslinking of DNA-protein complexes was reversed by incubation for 8 h at 65°C. DNA was extracted with a QIAquick PCR Purification Kit (QIAGEN, Hilden, Germany). DNA sequencing was performed on an Illumina HiSeq 2000 instrument using TruSeq Rapid SBS Kits (Illumina, San Diego, CA, USA, FC-402-4002) in accordance with the manufacturer's protocols. ChIP-enriched DNA fragments were mapped based on the Human Feb 2009 assembly and visualized using the UCSC Genome Browser. The mapped ChIP-Seq data were subjected to peak calling with ChIP-Peak and subjected to further bioinformatics analysis. The ChIP-Seq experiments were performed by KangChen Biotech (KangChen, Shanghai, China). Gene-specific primers (Supplementary Table 1) were predesigned and synthesized for analysis of the captured DNA fragments via RT-PCR.

FBXW7-luciferase reporter assay

BGC-823 cells were plated into 96-well plates, with five wells per group. The pGL3-FBXW7-luc plasmid was amplified in DH5α cells and treated with the CpG methyltransferase M. SssI (M0226S, NEB, USA) for 48 h to construct the pGL3-FBXW7-luc + Methylation plasmid. Cells were then transfected separately with the pGL3-luc, pGL3-FBXW7-luc, and pGL3-FBXW7-luc + Methylation plasmids for 48 h. In a separate experiment, cells were first transfected with the pGL3-FBXW7-luc or pGL3-FBXW7-luc + Methylation plasmid and then transfected with NC-siRNA, si-MECP2-1, si-MECP2-2, the control vector, or the MECP2 overexpression plasmid or treated with dimethyl sulfoxide (DMSO), or the methylation inhibitor 5-aza-2'-deoxycytidine (Aza). Luciferase activity was examined 48 h posttransfection with a Dual-Luciferase Reporter Assay System (Promega, Madison,

WI). Each experiment was performed independently three times.

In vivo metastasis assay

MECP2 shRNA- or sh-Con-transfected BGC-823 cells (1×10^6) were injected into the tail veins of nude mice (Supplementary Table 5). Thirty days after injection, the mice were sacrificed, and the lungs were resected and collected. Bioluminescence images were acquired and analyzed using a Xenogen IVIS Spectrum imaging system (Xenogen, Alameda, CA, USA). All animal procedures were approved by the Institutional Animal Care and Use Committee of Xi'an Jiaotong University and were performed in accordance with the institutional guidelines. There were 4 mice in each group.

Western blot analysis and co-immunoprecipitation (co-IP)

Total protein from human GC cell lines and tissues was lysed with RIPA lysis buffer (Cell Signaling Technology, Boston, MA) supplemented with protease inhibitors (Roche, Indianapolis, IN, USA) to obtain whole-cell extracts. Nuclear proteins were extracted using a Nuclear and Cytoplasmic Extraction Kit (Thermo Fisher Scientific, Waltham, MA, USA) and a CelLytic™ NuCLEAR™ Extraction Kit (Sigma, St. Louis, MO, USA) according to the manufacturers' instructions. Protein concentrations in the cellular and nuclear extracts were measured using a BCA Assay Kit (Thermo Fisher Scientific, Waltham, MA, USA). Protein extracts (25 μg) were separated by 10% sodium dodecyl sulfate-polyacrylamide gel electrophoresis and transferred to PVDF membranes. The membranes were incubated first with primary antibodies at 4°C overnight and then with the corresponding secondary antibodies for 1 h at room temperature. After that, the membranes were incubated with ECL reagent (Pierce, Rockford, IL, USA) for detection by chemiluminescence. The luminescence signal was measured and recorded with a Syngene Gbox system (Syngene, Cambridge, UK). β-Actin was used as the loading control. The primary antibodies used are listed in Supplementary Table 4.

RIPA lysis buffer was applied to collect protein lysates from BGC-823 and MKN-45 cells. 1 mg lysates were incubated with the appropriate primary antibody (4 μg) for 4 h at 4°C followed by 1 h incubation with Protein-A Sepharose beads (GE Healthcare). The beads were gathered by centrifugation for 5 min at 900 g. Then, sample loading buffer was applied to resuspend the Sepharose beads-antigen-antibody complexes. The specimens were gathered for Western blot analysis after boiling for 5 min.

GEO and EMBL-EBI data analysis

To verify that MECP2 regulates FBXW7 in a public database, GEO (https://www.ncbi.nlm.nih.gov/geo/, Dataset: GSE57303, Platform ID: GPL570) [24] and EMBL-EBI (https://www.ebi.ac.uk/arrayexpress, Dataset: E-MTAB-1440, Platform ID: GPL8432-11703) [25] microarray data were collected, and the correlation between MECP2 and FBXW7 expression was analyzed by using simple linear regression.

Statistical analysis

All data were analyzed using GraphPad 7.0 (GraphPad Software, USA) and SPSS 19.0 (Abbott Laboratories, Chicago, IL, USA). The results are expressed as the mean ± SEM of at least 3 independent experiments. Student's t test was used for comparisons between two independent groups. One-way ANOVA followed by multiple comparisons using Dunnett's test was performed to analyze differences among more than two groups. The chi-square test was employed to evaluate the relationships between FBXW7 expression and clinicopathologic characteristics. Pearson correlation analysis was conducted to estimate the association of MECP2 with FBXW7. $P < 0.05$ was considered statistically significant.

Results

MECP2 is overexpressed in GC and closely related to clinicopathological characteristics

Analysis based on The Cancer Genome Atlas (TCGA) data identified significant overexpression of MECP2 in GC tissues ($P < 0.001$, **Figure 1A**). QRT-PCR analysis of GC tissue samples and paired adjacent normal gastric tissue samples collected from 166 patients with GC in this study revealed markedly upregulated MECP2 mRNA expression in cancer tissues ($P < 0.001$, **Figure 1B**). This result is consistent with that of our previous study, which was based on 76 GC

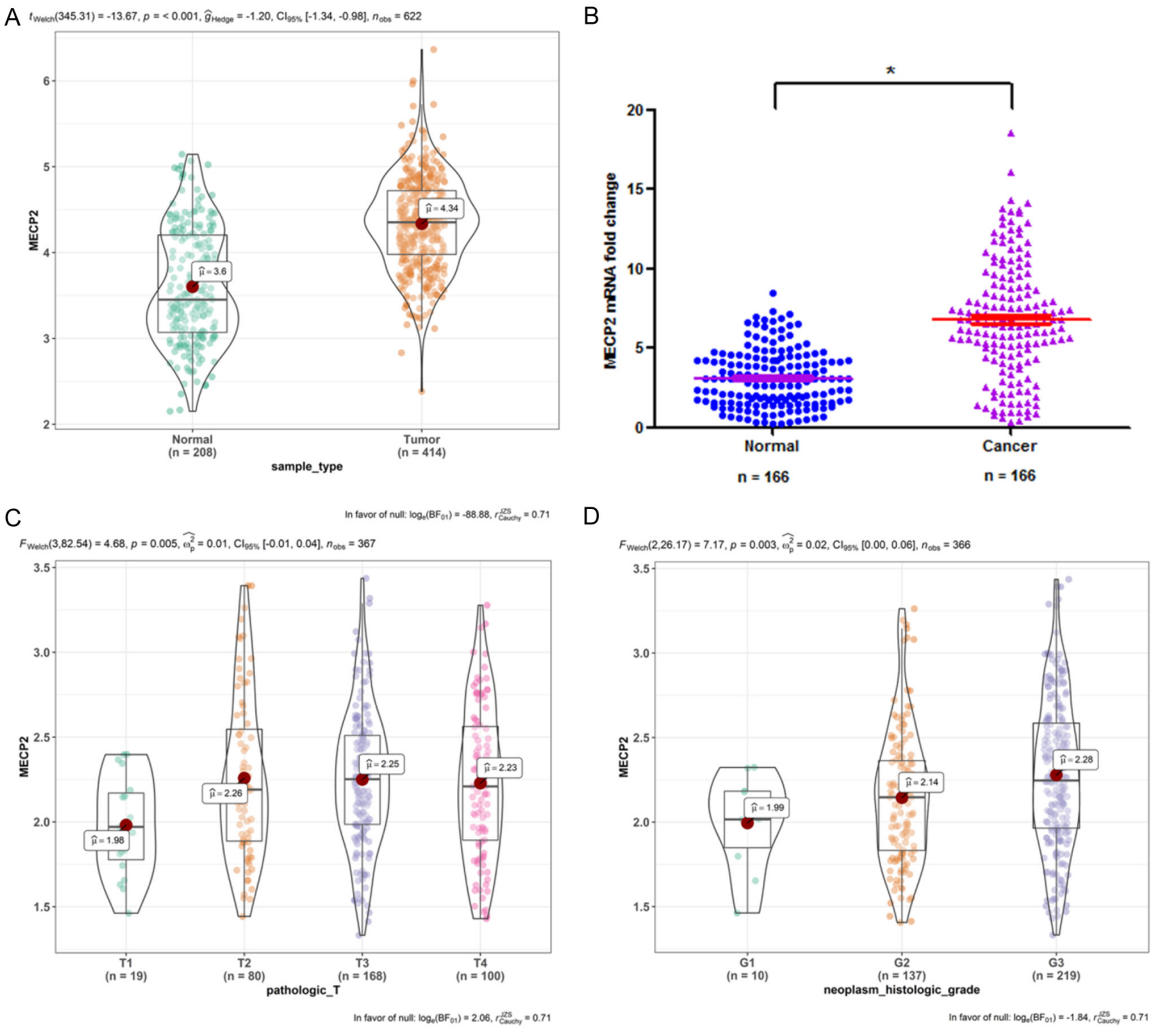

Figure 1. MECP2 is highly expressed in GC and correlated with the clinicopathologic characteristics of patients with GC. A. Analysis of MECP2 expression in tumor and normal tissues using TCGA data. B. Analysis of MECP2 mRNA expression in tumor and normal tissues by qRT-PCR. n = 166, *P < 0.001. C. Correlation between MECP2 expression and tumor histology based on TCGA data. The data are shown as the means ± SEMs (P < 0.01, chi-square test). D. Correlation between MECP2 expression and T stage based on TCGA data. The data are shown as the means ± SEMs (*P < 0.01, chi-square test).

patients [21]. Further analysis suggested correlations between MECP2 expression and clinicopathologic characteristics. High MECP2 expression was associated with histology, tumor size, lymph node metastasis, lymphatic invasion, serosal invasion and T stage (Supplementary Table 6). However, MECP2 expression was not associated with age, sex, venous invasion, or liver metastasis. Analysis of TCGA data also revealed an association of high MECP2 expression with unfavorable tumor histology and higher T stage (P < 0.01, **Figure 1C**, **1D**).

MECP2 facilitates the migration and invasion of GC cells

To investigate the causal role of MECP2 in GC progression, an MECP2 overexpression plasmid was constructed, and MECP2-targeting siRNAs (si-MECP2-1 and si-MECP2-2) were designed and synthesized. QRT-PCR showed that the MECP2 overexpression plasmid observably upregulated the mRNA expression of MeCP2 in BGC-823 and MKN-45 cells (P < 0.001, **Figure 2A**), while si-MECP2-1 and si-MECP2-2 significantly downregulated MeCP2 mRNA expres-

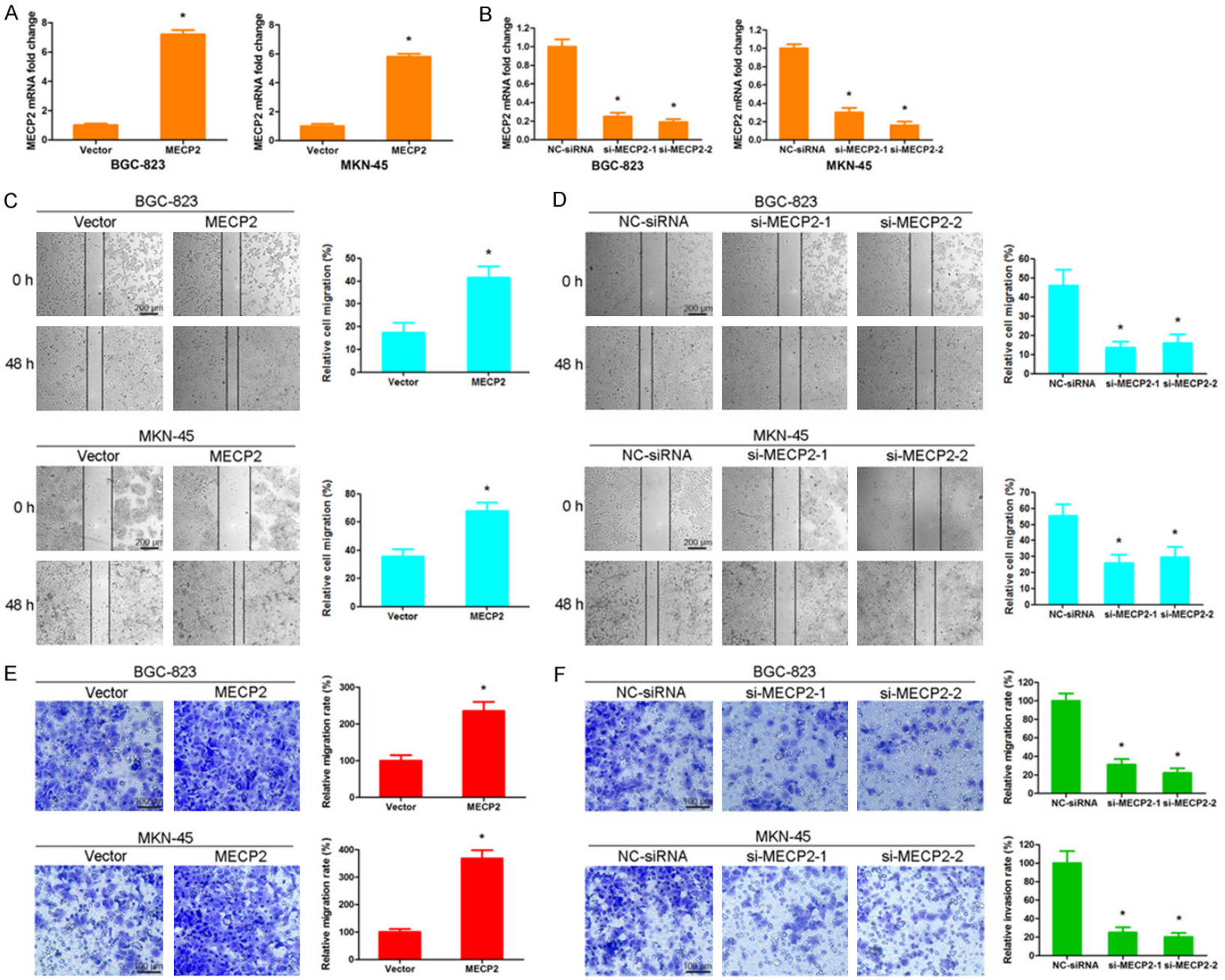
A
MECP2 mRNA fold change
Vector
MECP2
BGC-823
MKN-45
B
NC-siRNA
si-MECP2-1
si-MECP2-2
C
D
0 h
48 h
Relative cell migration (%)
E
F
Relative migration rate (%)
Relative invasion rate (%)

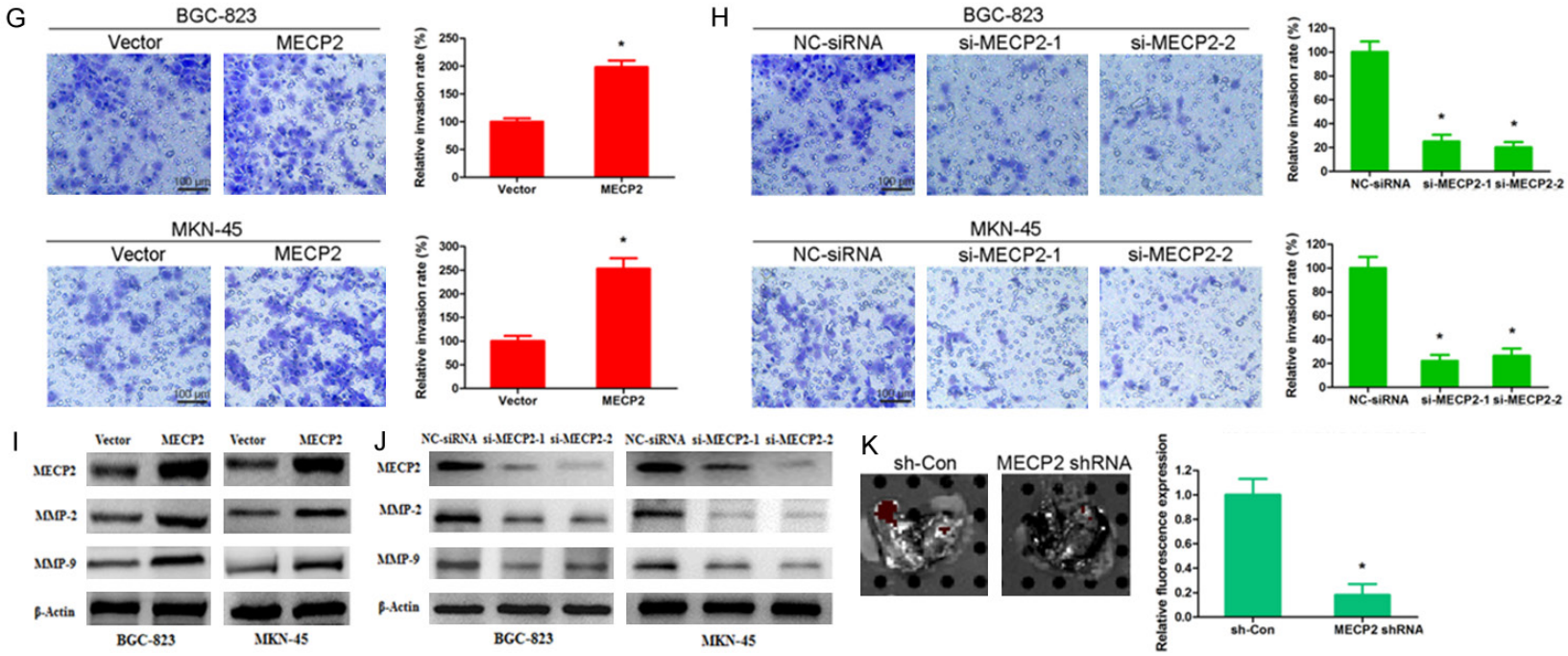

Figure 2. MECP2 promotes GC cell migration and invasion. A. MECP2 mRNA expression in BGC-823 and MKN-45 cells 24 h after transfection with the MECP2 overexpression plasmid. *P < 0.001. B. MECP2 mRNA expression in BGC-823 and MKN-45 cells 24 h after transfection with MECP2 siRNAs. *P < 0.001. C. Wound healing assay. The MECP2 overexpression plasmid promoted cell migration 48 h after transfection. *P < 0.01. D. Si-MECP2-1 and si-MECP2-2 inhibited cell migration. *P < 0.01. E. Transwell migration assay. The MECP2 overexpression plasmid enhanced cell migration. *P < 0.01. F. Si-MECP2-1 and si-MECP2-2 inhibited cell migration. *P < 0.01. G. Transwell invasion assay. The MECP2 overexpression plasmid promoted cell invasion. *P < 0.01. H. si-MECP2-1 and si-MECP2-2 suppressed cell invasion. *P < 0.01. I. The MECP2 overexpression plasmid upregulated the protein expression of MECP2, MMP-2 and MMP-9. J. Si-MECP2-1 and si-MECP2-2 downregulated the protein expression of MECP2, MMP-2 and MMP-9. n = 3. K. Representative images of metastatic foci formed in the lungs after injection of MECP2 shRNA or sh-Con cells are shown. n = 4, *P < 0.01.

sion ($P < 0.001$, **Figure 2B**). Immunofluorescence staining revealed a higher level of exogenous MECP2 protein in the GFP-MECP2-vector group than in the GFP-vector group in both BGC-823 and MKN-45 cells (Supplementary Figure 1A, 1B). Our previous study demonstrated that MECP2 promoted the proliferation and inhibited the apoptosis of GC cells [21, 22]. To further study the effect of MECP2 on GC progression, a wound healing assay and Transwell migration and invasion assays were performed to explore the effect of MECP2 on the migration and invasion abilities of GC cells. The wound healing assay showed that the MECP2 overexpression plasmid significantly enhanced the migration of BGC-823 GC and MKN-45 cells into the scratched area, while si-MECP2-1 and si-MECP2-2 markedly suppressed cell migration ($P < 0.01$, **Figure 2C**, **2D**). Consistent with these results, the Transwell assays also revealed a promoting effect of the MECP2 overexpression plasmid and an inhibitory effect of si-MECP2-1 and si-MECP2-2 on cell migration ($P < 0.01$, **Figure 2E**, **2F**). Moreover, the MECP2 overexpression plasmid markedly promoted cell invasion, and si-MECP2-1 and si-MECP2-2 significantly inhibited cell invasion ($P < 0.01$, **Figure 2G**, **2H**). Further exploration of the molecular mechanism by which MECP2 modulates GC progression revealed that the protein expression levels of MECP2, MMP-2 and MMP-9 were increased by the MECP2 overexpression plasmid but downregulated by si-MECP2-1 and si-MECP2-2 (**Figure 2I**, **2J**). To further assess the role of MECP2 in GC metastasis in vivo, we established a tail vein metastasis model by injecting BGC-823 GC cells into nude mice. The results showed that MECP2 shRNA treatment significantly suppressed lung metastasis of GC cells in vivo ($P < 0.01$, **Figure 2K**). These data suggested that MECP2 might promote the migration and invasion of GC cells by regulating MMP-2 and MMP-9 expression.

MECP2 suppresses FBXW7 transcription by binding to its promoter

To explore how MECP2 might regulate GC cell migration and invasion, a ChIP-Seq assay was performed with BGC-823 cells to identify the genes regulated by MECP2. In total, 8129 ChIP-Seq peaks with various fold enrichment were acquired, among which 220 were located in the promoter regions of genes. Then, MethPrimer was used to predict potential CpG sites within the MECP2 binding regions. The results showed that the MECP2 binding region in the promoter of FBXW7 contained a CpG site (Cg01181485, **Figure 3A**). The ChIP-qPCR results also verified that MECP2 can directly bind to the promoter of FBXW7 (**Figure 3B**). Wild-type (WT) and mutant (MT) GFP-MECP2 plasmids were constructed. After they were transfected into BGC-823 cells, we performed ChIP-qPCR with an anti-GFP antibody. The findings revealed that exogenous MECP2 can also bind to the CpG site in the FBXW7 promoter region (**Figure 3C**). No binding to this site was detected in cells transfected with the GFP plasmid (Ctrl), GFP-MT1 plasmid or GFP-MT2 plasmid, but binding was detected in cells transfected with the GFP-WT plasmid (**Figure 3D**). Analysis of TCGA data showed that the methylation level of the CpG site (Cg0118-1485) was inversely correlated with the expression level of FBXW7 in GC cells ($P < 0.01$, **Figure 3E**).

Subsequently, a promoter reporter assay was performed to determine whether MECP2 can bind to the CpG site in the promoter region of FBXW7. The sequences of the binding sites in the FBXW7 promoter region identified by ChIP-Seq were subcloned upstream of the luciferase gene in the pGL3 reporter plasmid (Supplementary Table 7). Luciferase activity in BGC-823 cells was measured 48 h after transfection with different plasmids. Luciferase activity was evidently reduced in the pGL3-FBXW7-luc and pGL3-FBXW7-luc + Methylation groups compared with the pGL3 group, and luciferase activity in the pGL3-FBXW7-luc + Methylation group was significantly lower than that in the pGL3-FBXW7-luc group ($P < 0.01$, **Figure 3F**). Among the groups transfected first with the pGL3-FBXW7-luc plasmid and then transfected with NC-siRNA, si-MECP2-1, si-MECP2-2, the control vector, or the MECP2 overexpression plasmid or treated with dimethyl sulfoxide (DMSO), or the methylation inhibitor 5-aza-2'-deoxycytidine (Aza), luciferase activity was observably enhanced in the si-MECP2-1 and si-MECP2-2 groups compared with the NC-siRNA group, markedly increased in the 5-aza-2'-deoxycytidine (Aza) group compared with the DMSO group, and significantly decreased in the MECP2 overexpression plasmid group compared with the control vector group. The groups first transfected with the pGL3-FBXW7-luc + Methylation plasmid and then subjected to further treatment exhibited similar results in lucif-

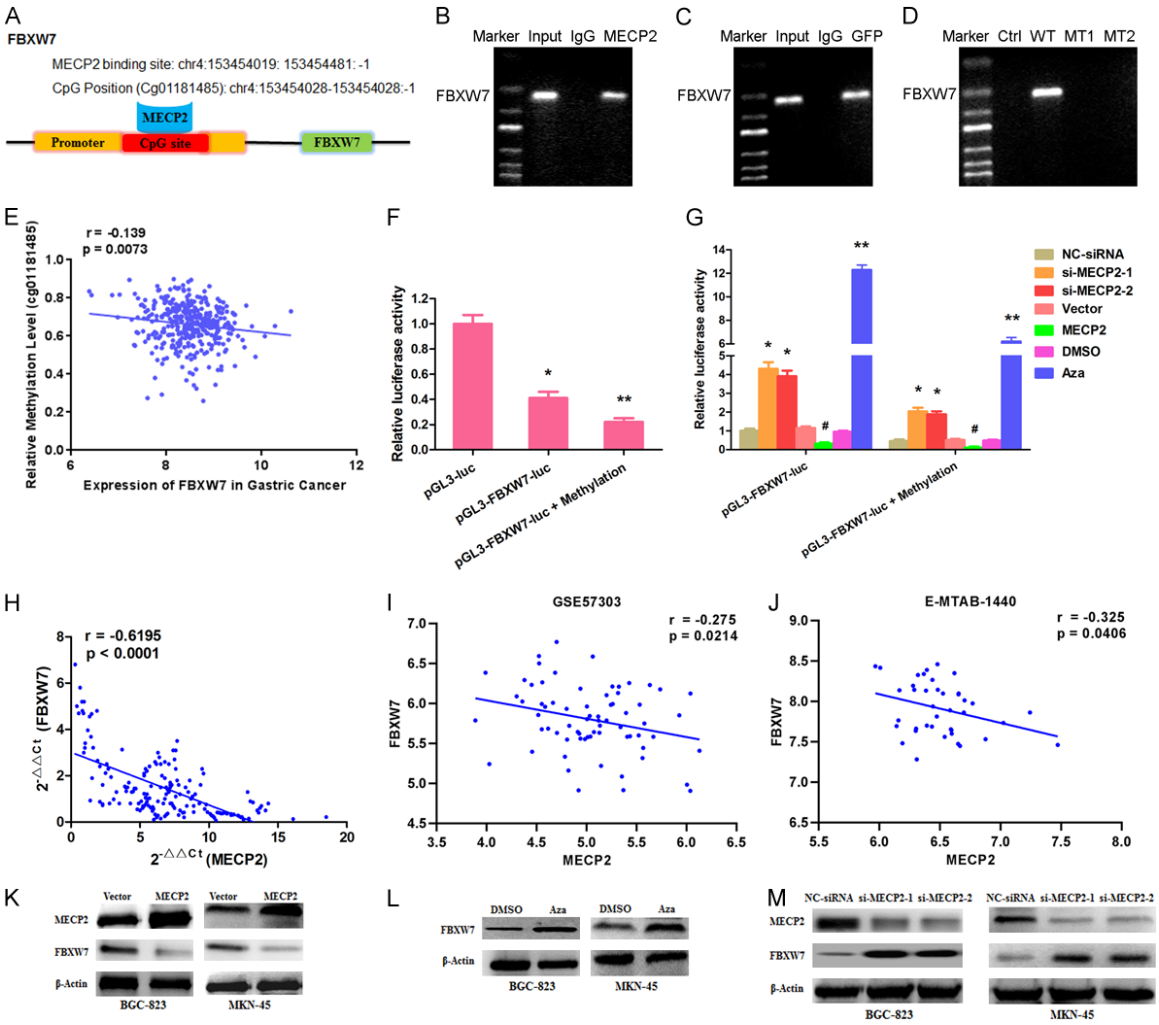

Figure 3. MECP2 inhibits FBXW7 expression in GC cells by binding to the promoter region of FBXW7. A. MECP2 ChIP-Seq assay and MethPrimer data. MECP2 bound to the CpG site in the promoter region of FBXW7. B. ChIP-qPCR analysis of FBXW7 with an anti-MECP2 antibody. C. ChIP-qPCR analysis of FBXW7 with an anti-GFP antibody after transfection with the GFP-MECP2 plasmid. D. ChIP-qPCR analysis of FBXW7 with an anti-GFP antibody after transfection with the GFP plasmid (Ctrl), GFP-Mutation type 1 plasmid (MT1), GFP-Mutation type 2 plasmid (MT2), or GFP-MECP2 plasmid (WT). E. The methylation level of the CpG site (Cg01181485) was negatively correlated with the FBXW7 expression level in GC data from TCGA. r = -0.139, P = 0.0073, Pearson correlation analysis. F. Luciferase activity in BGC-823 cells was measured 48 h after transfection with the pGL3-FBXW7-luc plasmid (containing the target sequence in the promoter region of FBXW7) or the pGL3-FBXW7-luc + Methylation plasmid. Renilla luciferase served as the internal control. *P < 0.01 compared with pGL3-luc, #P < 0.01 compared with pGL3-FBXW7-luc. G. Luciferase activity in BGC-823 cells after transfection with the pGL3-FBXW7-luc plasmid, the pGL3-FBXW7-luc + Methylation plasmid, si-MECP2-1, si-MECP2-2, or the MECP2 overexpression plasmid or treatment with the methylation inhibitor 5-aza-2'-deoxycytidine (Aza). *P < 0.01 compared with NC-siRNA, **P < 0.01 compared with DMSO, #P < 0.01 compared with vector. H. Negative correlation between MECP2 and FBXW7 levels. The $2^{-\Delta\Delta Ct}$ values of MECP2 and FBXW7 mRNA expression were used for Pearson correlation analysis (r = -0.6195, n = 166, *P < 0.0001). I. MECP2 expression was negatively correlated with FBXW7 expression in GC data from GEO. r = -0.275, P = 0.0214, n = 70. J. MECP2 expression was negatively correlated with FBXW7 expression in GC data from EMBL-EBI. r = -0.325, P = 0.0406, n = 40. K. Western blot analysis of FBXW7 protein expression in BGC-823 and MKN-45 cells after transfection with the MECP2 overexpression plasmid. L. FBXW7 protein expression after treatment with the methylation inhibitor Aza. M. FBXW7 protein expression after transfection with si-MECP2-1 and si-MECP2-2. n = 3.

erase activity, but the activity was lower than that in the pGL3-FBXW7-luc groups (P < 0.01, **Figure 3G**). The MECP2 mRNA level was significantly negatively correlated with the FBXW7 mRNA level in GC tissues (r = -0.6195, P < 0.0001, Pearson correlation analysis; **Figure**

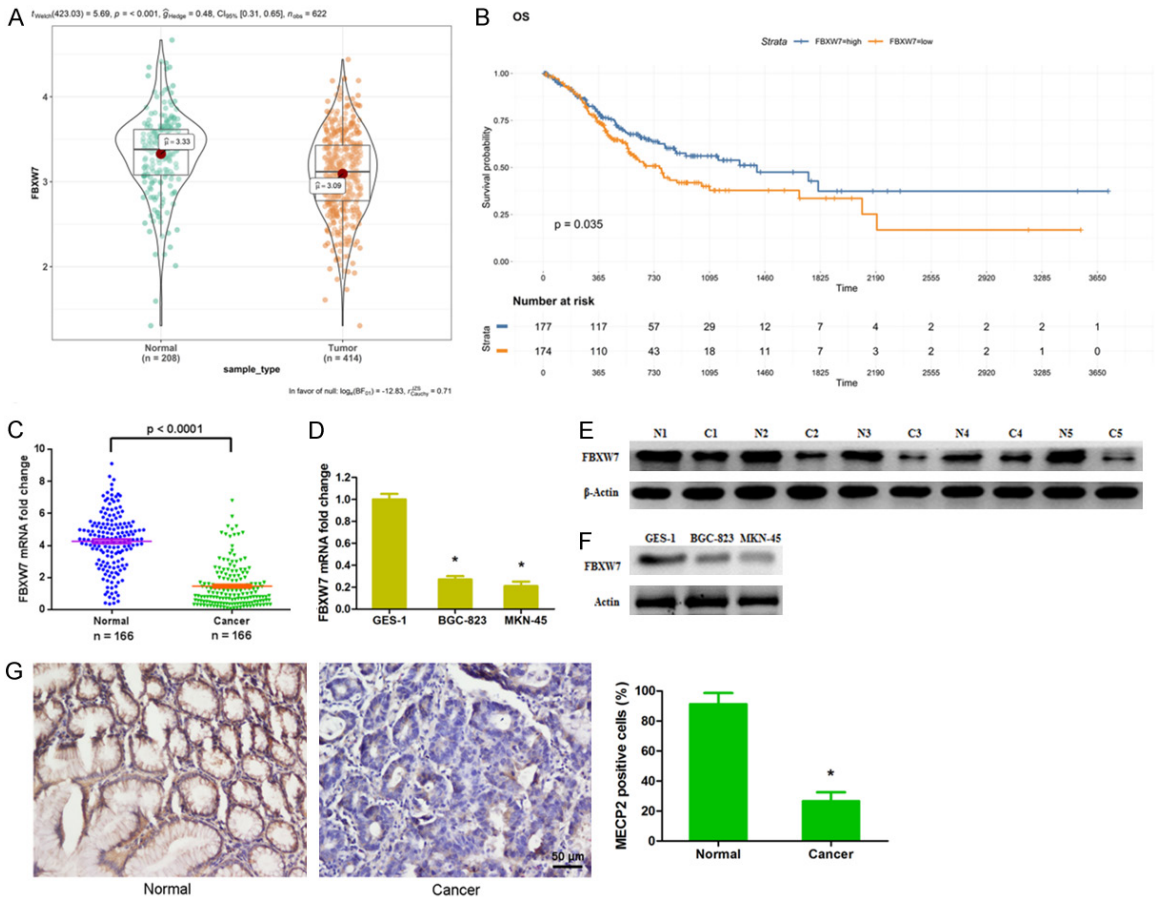

Figure 4. FBXW7 expression is downregulated in human GC tissues and cell lines. A. FBXW7 expression in tumor and normal tissues was analyzed using TCGA data. B. Kaplan-Meier curves of overall survival based on MeCP2 expression in TCGA data. C. FBXW7 mRNA expression in tumor and normal tissues. n = 166, *P < 0.0001. D. FBXW7 mRNA expression in GC cell lines (BGC-823 and MKN-45) and a normal human gastric epithelial cell line (GES-1). n = 3, *P < 0.001. E. FBXW7 protein expression in GC tissues was measured by Western blotting. β-Actin was used as the internal control. n = 5. F. FBXW7 protein expression in BGC-823 and MKN-45 GC cells and GES-1 cells. n = 3. G. FBXW7 protein expression in tumor and normal tissues was evaluated by immunohistochemical staining. Scale bars = 50 μm. n = 166.

3H). Analysis of GEO and EMBL-EBI data also showed that MECP2 expression was negatively correlated with FBXW7 expression in GC ($P < 0.05$, **Figure 3I**, **3J**). Furthermore, FBXW7 mRNA expression in BGC-823 and MKN-45 cells was markedly decreased after transfection with the MECP2 overexpression plasmid and increased after treatment with the methylation inhibitor Aza, si-MECP2-1 or si-MECP2-2 (Supplementary Figure 2A-C). The protein expression of FBXW7 in the cells was also inhibited by transfection of the MECP2 overexpression plasmid (**Figure 3K**) but was promoted by treatment with the methylation inhibitor Aza, si-MECP2-1 or si-MECP2-2 (**Figure 3L**, **3M**). These findings suggested that MECP2 is a transcriptional regulator of FBXW7 in GC cells.

FBXW7 is frequently downregulated in GC and is correlated with clinicopathologic features

To further verify the above findings, FBXW7 expression in the tissue samples was measured. Analysis of TCGA data revealed marked downregulation of FBXW7 expression in GC tissues compared with normal gastric tissues ($P < 0.001$, **Figure 4A**). In line with this, our statistical analyses showed that patients with lower FBXW7 levels had poorer overall survival ($P < 0.05$, **Figure 4B**). The mRNA expression of FBXW7 was significantly downregulated in GC tissues ($P < 0.0001$, **Figure 4C**). This trend was further verified by measuring FBXW7 expression in BGC-823 and MKN-45 GC cells. The mRNA expression of FBXW7 in BGC-823 and

Table 1. Patient characteristics and clinicopathologic correlation of FBXW7 expression in GC

Characteristics	Number of cases	FBXW7 protein expression		*P*-value
		High (n = 45)	Low (n = 121)	
Age				0.736
≥ 60 years	75	18	57	
< 60 years	91	27	64	
Sex				0.315
Male	102	24	78	
Female	64	21	43	
Histology				0.382
Well	86	21	65	
Moderate	32	13	19	
poor	48	11	37	
Size				0.0005*
< 50 mm	77	33	44	
≥ 50 mm	89	12	77	
Lymph node metastasis				0.0001*
Absent	58	35	23	
Present	108	10	98	
Lymphatic invasion				0.0008*
Absent	54	29	25	
Present	112	16	96	
Venous invasion				0.031*
Absent	93	32	61	
Present	73	13	60	
Serosal invasion				0.0007*
Absent	57	28	29	
Present	109	17	92	
Liver metastasis				0.208
Absent	124	37	87	
Present	42	8	34	
TNM Stage				0.0024*
I	31	16	15	
II	46	15	31	
III	57	10	47	
IV	32	4	28	

*P < 0.05.

MKN-45 cells was evidently lower than that in normal human gastric epithelial cells (GES-1) (P < 0.001, **Figure 4D**). Western blot analysis also revealed decreased FBXW7 protein expression in GC tissues in 5 pairs of GC and adjacent normal tissues, as well as in BGC-823 GC and MKN-45 cells (**Figure 4E**, **4F**). IHC staining revealed that the protein expression of FBXW7 was markedly lower in GC tissues than in normal gastric tissues (**Figure 4G**). Our data also showed that FBXW7 expression and the clinicopathologic characteristics of GC patients were correlated. Low FBXW7 expression was associated with larger tumor size (≥ 50 mm: 86.5%; < 50 mm: 57.1%), the presence of lymph node metastasis (absent: 39.7%; present: 90.7%), the presence of lymphatic invasion (absent: 46.3%; present: 85.7%), the presence of venous invasion (absent: 65.6%; present: 82.2%), the presence of serosal invasion (absent: 50.9%; present: 84.4%), and higher TNM stage (I: 48.4%; II: 67.4%; III: 82.5%; IV: 87.5%; **Table 1**). FBXW7 expression was not associated with age, sex, histology, or liver metastasis status.

MECP2 upregulates the Notch1/c-Myc/mTOR signaling pathways by repressing FBXW7 transcription

To investigate the potential molecular mechanisms by which MECP2 regulates GC cell migration and invasion, the mRNA and protein levels of FBXW7-related downstream genes were measured by qRT-PCR and Western blotting, respectively. FBXW7 is a substrate recognition subunit of the SKP1-CUL1-F-box protein (SCF) E3 ubiquitin ligase complex, which plays a crucial role in tumorigenesis and cancer progression by promoting the ubiquitination-mediated degradation of oncoproteins, including mTOR, c-Myc, c-Jun, and Notch1 [26-28]. The endogenous co-IP demonstrated that Notch1, c-Myc and mTOR interacted with FBXW7 in BGC-823 and MKN-45 GC cells (Supplementary Figure 4A). The results of qRT-PCR showed that the mRNA expression levels of Hes1, MMP-2 and MMP-9 in BGC-823 and

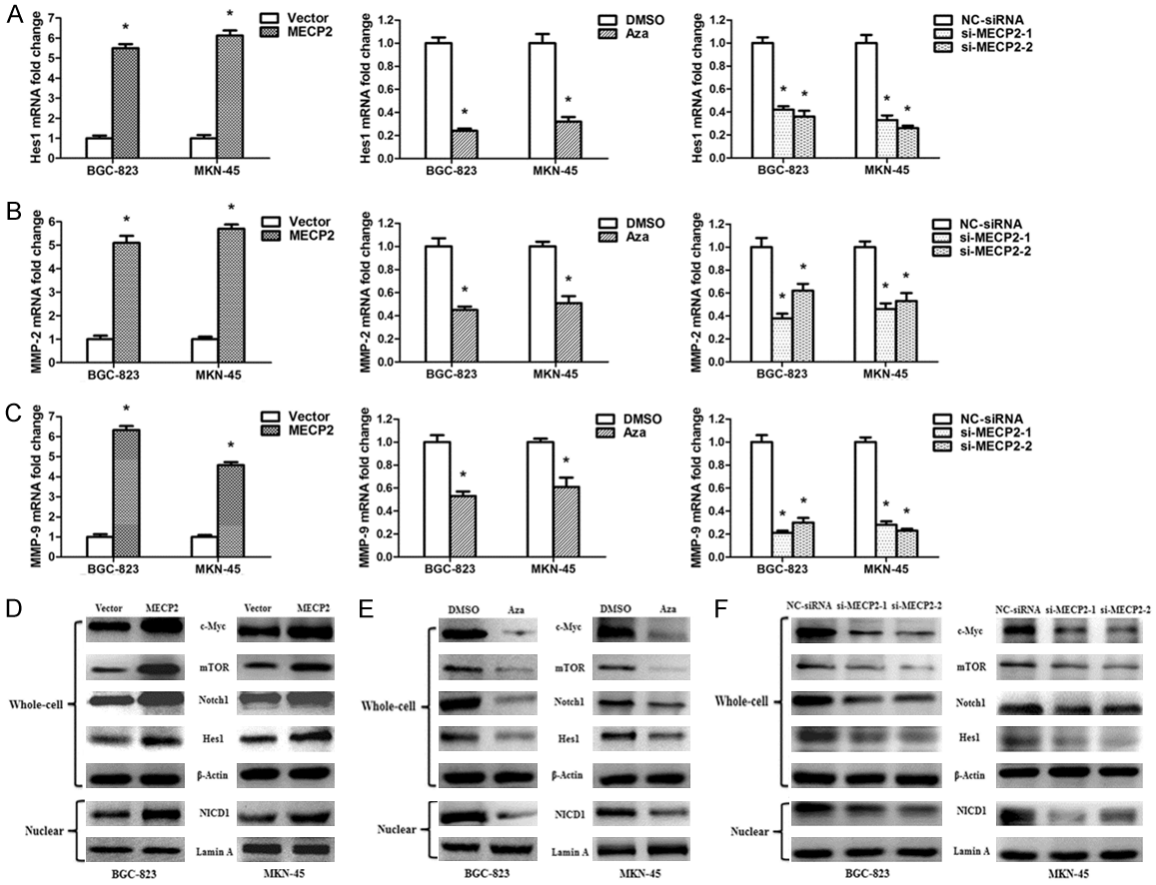

Figure 5. MECP2 regulates the Notch1/c-Myc/mTOR signaling pathways in human GC cells by inhibiting FBXW7 expression. A. Hes1 mRNA expression in BGC-823 and MKN-45 cells after transfection with the MECP2 overexpression plasmid, MECP2-1, or si-MECP2-2 or treatment with the methylation inhibitor Aza. *P < 0.001. B. MMP-2 mRNA expression in GC cells after treatment. *P < 0.001. C. MMP-9 mRNA expression in GC cells after treatment. *P < 0.001. D. The expression of proteins related to the Notch1/c-Myc/mTOR signaling pathways after transfection with the MECP2 overexpression plasmid. E. The expression of proteins related to the Notch1/c-Myc/mTOR signaling pathways after treatment with the methylation inhibitor Aza. F. The expression of proteins related to the Notch1/c-Myc/mTOR signaling pathways after transfection with si-MECP2-1 and si-MECP2-2. n = 3.

MKN-45 cells increased significantly after transfection with MECP2 overexpression plasmid and decreased dramatically after treatment with the methylation inhibitor Aza, si-MECP2-1, or si-MECP2-2 (P < 0.001, **Figure 5A-C**). However, there were no significant differences in the mRNA levels of c-Myc, mTOR and Notch1 after these treatments (Supplementary Figure 3A-C). Western blot analysis revealed that the whole-cell protein expression levels of c-Myc, mTOR, Notch1, Hes1, MMP-2 and MMP-9 were increased after transfection with the MECP2 overexpression plasmid and decreased after treatment with the methylation inhibitor Aza, si-MECP2-1 or si-MECP2-2 (**Figure 2I**, **2J**; **Figure 5D-F**). In addition, the change in the nuclear NICD1 protein level was consistent with the change in the whole-cell Notch1 protein level (**Figure 5D-F**). MECP2 mRNA expression was significantly positively correlated with the protein expression of c-MYC, mTOR and Notch1 in human GC tissues (P < 0.01, Supplementary Figure 4B-D). Based on these findings, MECP2 might regulate the Notch1/c-Myc/mTOR signaling pathways by inhibiting the ubiquitination-mediated degradation of Notch1, c-Myc and mTOR by suppressing FBXW7 transcription in GC cells.

FBXW7 inhibits GC cell migration and invasion by regulating the Notch1/c-Myc/mTOR signaling pathways

Since MECP2 was found to regulate GC cell migration and invasion and FBXW7 was confirmed as a target gene of MECP2, overexpres-

sion and knockdown of FBXW7 were performed in GC cell lines to verify its involvement in the oncogenic function of MECP2. The wound healing assay revealed that the FBXW7 overexpression plasmid substantially suppressed the migration of cells into the wounded area in BGC-823 and MKN-45 GC cells, but si-FBXW7-1 and si-FBXW7-2 significantly promoted GC cell migration ($P < 0.01$, **Figure 6A**, **6B**). The Transwell assays also showed that the FBXW7 overexpression plasmid markedly suppressed GC cell migration and si-FBXW7-1 and si-FBXW7-2 strikingly promoted GC cell migration ($P < 0.01$, **Figure 6C**, **6D**). Moreover, the FBXW7 overexpression plasmid significantly inhibited cell invasion, while si-FBXW7-1 and si-FBXW7-2 markedly enhanced GC cell invasion ($P < 0.01$, **Figure 6E**, **6F**). Then, the downstream mechanism of FBXW7 regulation was further explored. QRT-PCR analysis showed that the FBXW7 overexpression plasmid appreciably increased FBXW7 mRNA expression in BGC-823 and MKN-45 cells ($P < 0.001$, **Figure 6G**), while si-FBXW7-1 and si-FBXW7-2 markedly decreased FBXW7 mRNA expression ($P < 0.001$, **Figure 6H**). No significant differences were observed in the levels of c-Myc, mTOR and Notch1 after transfection with the FBXW7 overexpression plasmid, si-FBXW7-1 or si-FBXW7-2 (Supplementary Figure 5A-C). The mRNA levels of Hes1, MMP-2 and MMP-9 in the cells were markedly decreased after transfection with the FBXW7 overexpression plasmid and obviously increased after transfection with si-FBXW7-1 and si-FBXW7-2 ($P < 0.001$, Supplementary Figure 5D-F). Western blot analysis showed that the FBXW7 overexpression plasmid upregulated FBXW7 protein expression, while si-FBXW7-1 and si-FBXW7-2 downregulated FBXW7 protein expression. In addition, the whole-cell protein expression levels of c-Myc, mTOR, Notch1, Hes1, MMP-2 and MMP-9 were reduced after transfection with the FBXW7 overexpression plasmid but increased after transfection with si-FBXW7-1 and si-FBXW7-2. The change in the nuclear NICD1 protein level was consistent with that in the whole-cell Notch1 protein level (**Figure 6I**, **6J**).

Knockdown of FBXW7 reverses the effect of MECP2 silencing on GC cells

To further confirm that MECP2 promotes GC cell migration and invasion by suppressing FBXW7 expression, FBXW7 siRNA was cotransfected with MECP2 siRNA into BGC-823 and MKN-45 cells. The wound healing assay showed that silencing MECP2 inhibited GC cell migration and that this effect was abolished by knockdown of FBXW7 ($P < 0.01$, **Figure 7A**). The Transwell assays also revealed that silencing MECP2 suppressed cell migration and that this suppression was reversed after cotransfection with MECP2 siRNA and FBXW7 siRNA ($P < 0.01$, **Figure 7B**). In addition, cotransfection with MECP2 siRNA and FBXW7 siRNA rescued the effect of MECP2 knockdown on cell invasion ($P < 0.01$, **Figure 7C**). The downstream regulators involved in the promotion of cell migration and invasion by MECP2 were analyzed by qRT-PCR. MECP2 mRNA expression was significantly decreased in BGC-823 and MKN-45 cells after transfection with MECP2 siRNA or MECP2 siRNA + FBXW7 siRNA ($P < 0.01$, **Figure 7D**). The mRNA expression of FBXW7 was markedly increased after transfection with MECP2 siRNA, and this effect was abolished by transfection with MECP2 siRNA + FBXW7 siRNA ($P < 0.01$, **Figure 7E**). The mRNA levels of c-Myc, mTOR and Notch1 did not differ significantly among cells transfected with MECP2 siRNA alone, cells cotransfected with MECP2 siRNA + FBXW7 siRNA, and cells transfected with NC-siRNA (Supplementary Figure 6A-C). Silencing MECP2 decreased the mRNA levels of Hes1, MMP-2 and MMP-9, while cotransfection with MECP2 siRNA and FBXW7 siRNA reversed these decreases ($P < 0.01$, Supplementary Figure 6D-F). The protein expression level of MECP2 was decreased in GC cells after transfection with MECP2 siRNA or MECP2 siRNA + FBXW7 siRNA. However, FBXW7 protein expression was increased after transfection with MECP2 siRNA, and transfection with MECP2 siRNA + FBXW7 siRNA reversed this increase. Knockdown of MECP2 also decreased the whole-cell protein expression levels of c-Myc, mTOR, Notch1, Hes1, MMP-2 and MMP-9. Compared with those in cells transfected with MECP2 siRNA alone, the protein expression levels of these genes were increased in cotransfected cells. Moreover, the change in the nuclear NICD1 protein level was consistent with that in the whole-cell protein level of Notch1 (**Figure 7F**). The above findings demonstrated that MECP2 promotes GC cell migration and invasion by inhibiting FBXW7 transcription, thereby

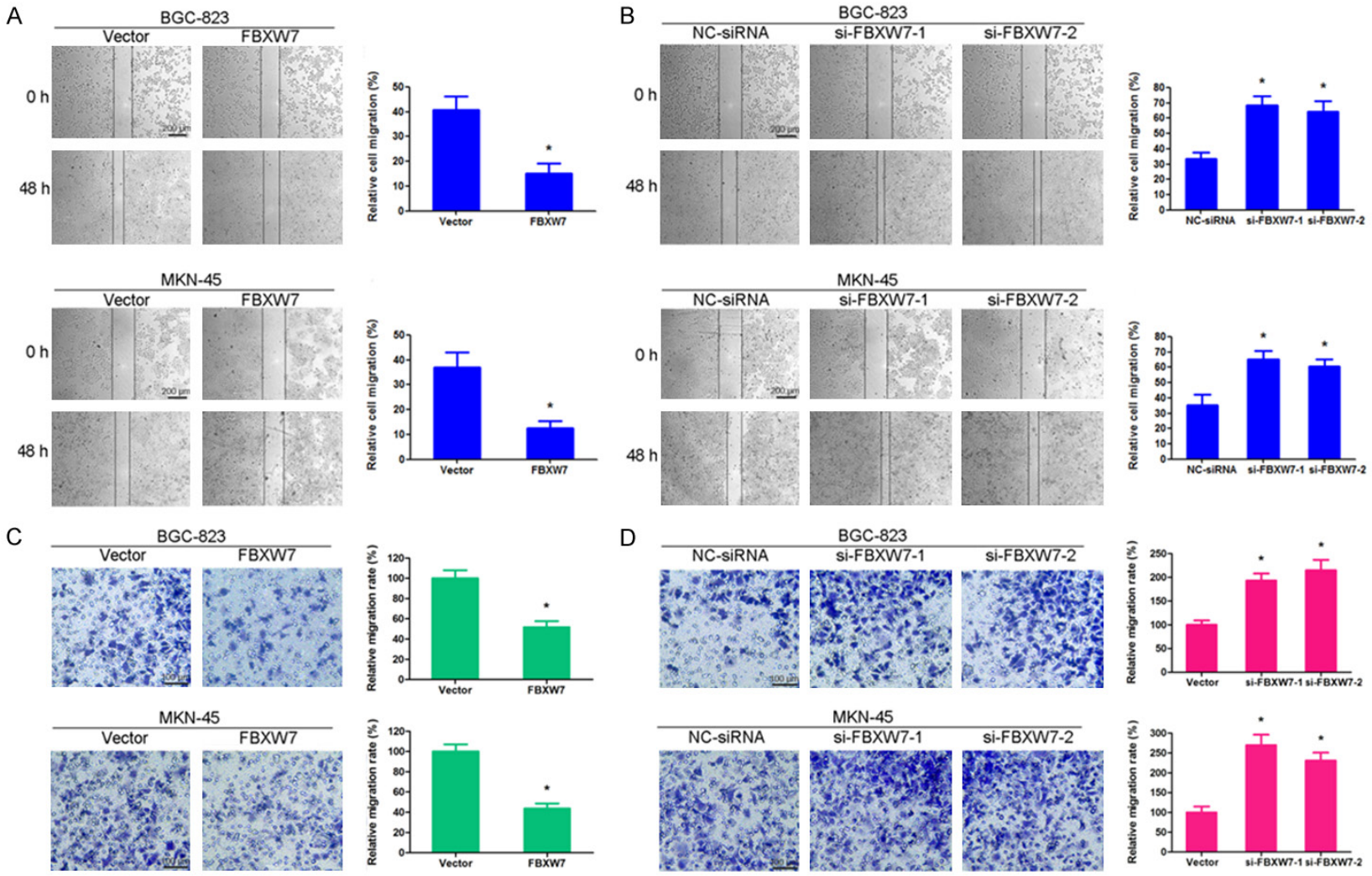
A
BGC-823
Vector
FBXW7
0 h
48 h
Relative cell migration (%)
Vector
FBXW7
MKN-45
Vector
FBXW7
0 h
48 h
Relative cell migration (%)
Vector
FBXW7
B
BGC-823
NC-siRNA
si-FBXW7-1
si-FBXW7-2
0 h
48 h
Relative cell migration (%)
NC-siRNA
si-FBXW7-1
si-FBXW7-2
MKN-45
NC-siRNA
si-FBXW7-1
si-FBXW7-2
0 h
48 h
Relative cell migration (%)
NC-siRNA
si-FBXW7-1
si-FBXW7-2
C
BGC-823
Vector
FBXW7
Relative migration rate (%)
Vector
FBXW7
MKN-45
Vector
FBXW7
Relative migration rate (%)
Vector
FBXW7
D
BGC-823
NC-siRNA
si-FBXW7-1
si-FBXW7-2
Relative migration rate (%)
Vector
si-FBXW7-1
si-FBXW7-2
MKN-45
NC-siRNA
si-FBXW7-1
si-FBXW7-2
Relative migration rate (%)
Vector
si-FBXW7-1
si-FBXW7-2

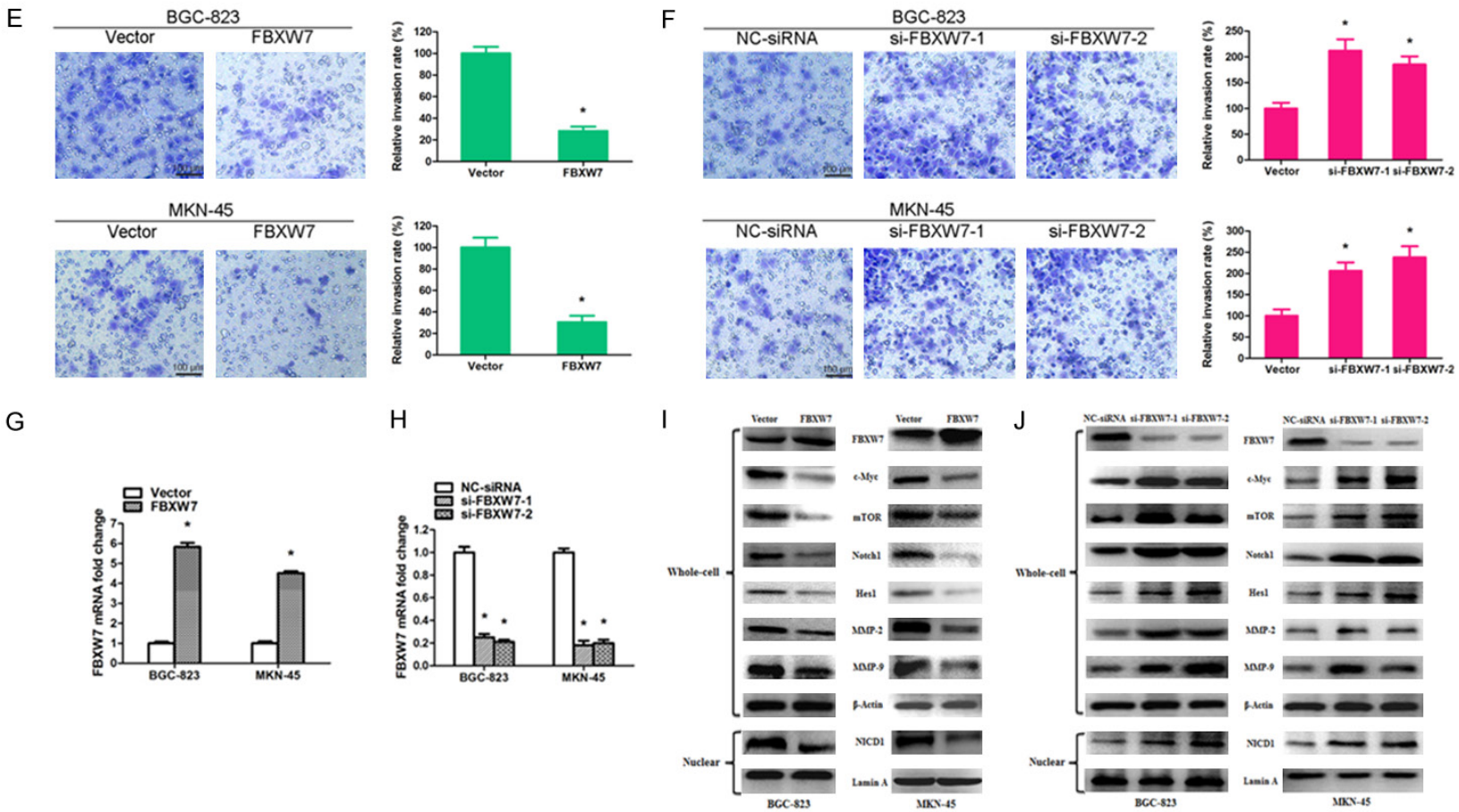

Figure 6. FBXW7 inhibits GC cell migration and invasion. A. Wound healing assay. The FBXW7 overexpression plasmid inhibited BGC-823 and MKN-45 cell migration 48 h after transfection. *P < 0.01. B. si-FBXW7-1 and si-FBXW7-2 promoted cell migration. *P < 0.01. C. Transwell migration assay. The FBXW7 overexpression plasmid repressed cell migration. *P < 0.01. D. si-FBXW7-1 and si-FBXW7-2 GC enhanced cell migration. *P < 0.01. E. Transwell invasion assay. The FBXW7 overexpression plasmid inhibited cell invasion. *P < 0.01. F. si-FBXW7-1 and si-FBXW7-2 promoted cell invasion. *P < 0.01. G. FBXW7 mRNA expression in GC cells 24 h after transfection with the FBXW7 overexpression plasmid. *P < 0.001. H. FBXW7 mRNA expression in GC cells 24 h after transfection with FBXW7 siRNAs. *P < 0.001. I. The FBXW7 overexpression plasmid downregulated the expression of proteins related to the Notch1/c-Myc/mTOR signaling pathways. J. si-FBXW7-1 and si-FBXW7-2 upregulated the expression of proteins related to the Notch1/c-Myc/mTOR signaling pathways. n = 3.

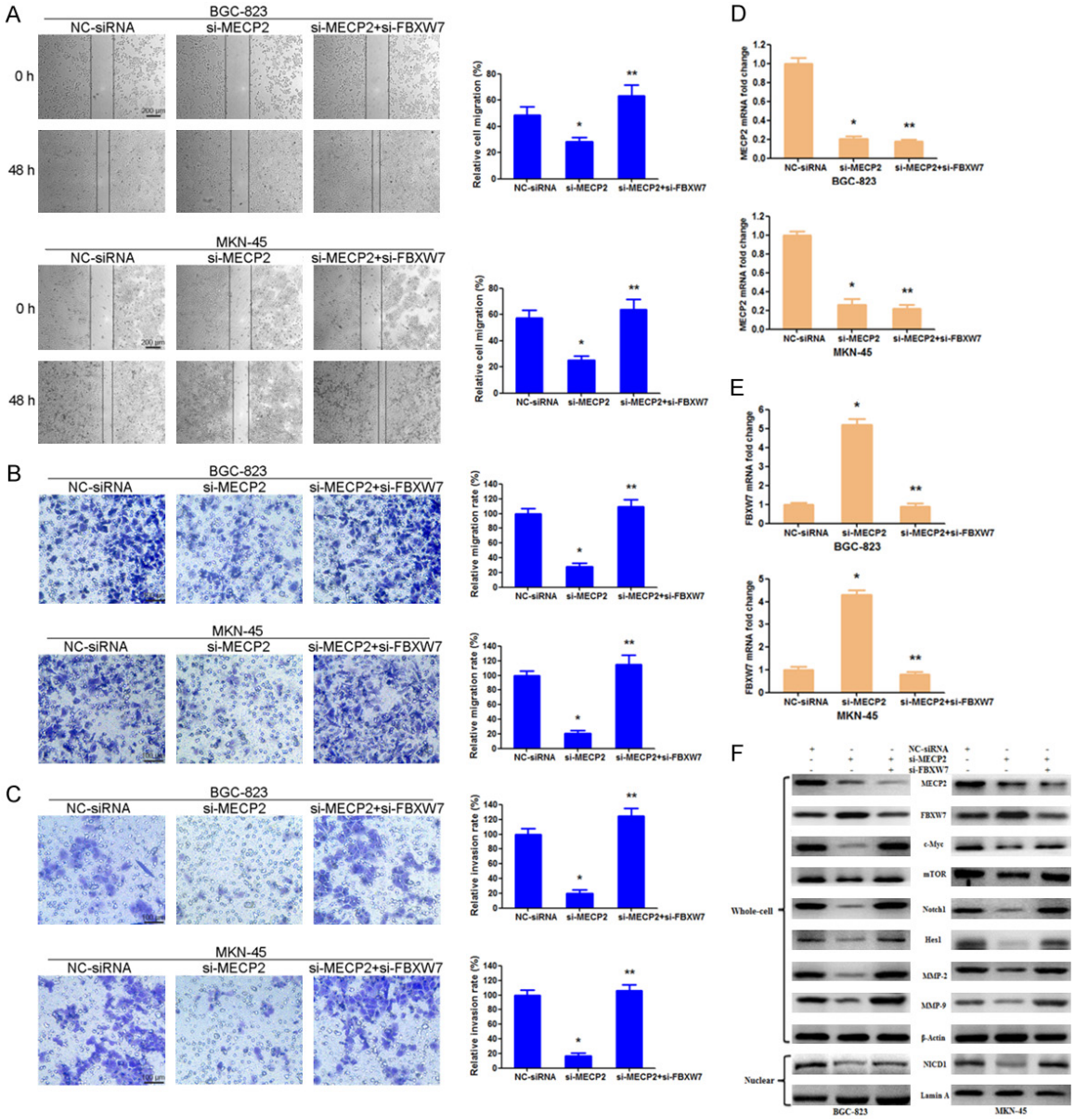

Figure 7. MECP2 promotes GC cell migration and invasion by upregulating the Notch1/c-Myc/mTOR signaling pathways through suppression of FBXW7 transcription. BGC-823 and MKN-45 cells were transfected with si-MECP2 alone or cotransfected with si-MECP2 and si-FBXW7. A. Wound healing assay. B. Transwell migration assay. C. Transwell invasion assay. D. MECP2 mRNA expression in cells 24 h after transfection. E. FBXW7 mRNA expression 24 h after transfection. F. The expression of proteins related to the Notch1/c-Myc/mTOR signaling pathways after transfection. *P < 0.01 compared with cells transfected with NC-siRNA; **P < 0.01 compared with cells transfected with si-MECP2. n = 3.

regulating the Notch1/c-Myc/mTOR signaling pathways.

Discussion

Tumorigenesis and tumor progression are multistep and multifactorial processes involving different genes that are accompanied by alterations in a variety of gene expression patterns that in turn affect cancer cell survival, growth, cycle, apoptosis, migration and invasion processes regulated by these genes [29]. In recent years, accumulating evidence has confirmed that MECP2, a key epigenetic regulator, plays an important oncogenic role in several cancer types [18, 30]. For example, MECP2 expression

is upregulated and promotes tumor progression in breast cancer, lung cancer, cervical cancer and uterine cancer [18]. MECP2 expression enhances oral squamous cell carcinoma and colorectal cancer growth and promotes tumorigenesis and tumor development in osteosarcoma and neuroblastoma [31, 32]. Silencing MECP2 reduces the proliferation of transformed human prostate cells [33]. Recent research has found that MECP2 regulates cancer cell migration and invasion in glioma and breast cancer [34, 35]. Our previous studies suggested that MECP2 promotes cell proliferation and the G1/S transition and suppresses apoptosis in liver cancer, gastric cancer and breast cancer [19-22]. By expanding the sample, the present study aims to further identify the effect of MECP2 on GC cell migration and invasion and determine the molecular mechanism. Our results again demonstrate that MECP2 expression is upregulated in primary GC and that high MECP2 expression is closely related to unfavorable tumor histology and high T stage. These findings suggest that MECP2 may play a key role in GC progression.

Our results demonstrated that high expression of MECP2 in GC cells significantly promoted their migration and invasion in vitro, while silencing MECP2 markedly suppressed cell migration and invasion by upregulating the expression of matrix metalloproteinase-2 (MMP-2) and MMP-9. Moreover, silencing MECP2 significantly inhibited lung metastasis of GC cells in vivo. The process of cancer metastasis is a multistep biochemical cascade involving many molecular events. An essential step of tumor invasion and metastasis is the degradation of matrix proteins, in which matrix metalloproteinases (MMPs) are the most crucial proteolytic enzymes. MMPs facilitate the access of cancer cells to the vasculature and their subsequent travel to target organs, where they form metastases by degrading the basement membrane and extracellular matrix (ECM) [36]. MMPs can also stimulate cancer cell proliferation and motility for development of metastases by enhancing the release of growth factors [37]. MMP-2 and MMP-9 can degrade type IV collagen, the major component of the basement membrane separating epithelial cells from the stroma [38, 39], and they have been reported to promote GC cell migration and invasion [40, 41]. Taking these observations together with the findings of the present study, we suggest that MECP2 facilitates GC cell migration and invasion by upregulating MMP-2/9 expression.

Our study identifies FBXW7 as an MECP2-targeting gene. MECP2 binds to the methylated CpG site in the promoter region of FBXW7, resulting in inhibition of FBXW7 transcription. This finding is consistent with that of some previous studies that showed that MECP2 functions as a transcriptional repressor by binding to the methylated CpG sites in gene promoter regions and recruiting corepressors (e.g., histone deacetylases and Sin3A) to repress the expression of some genes (e.g., MYOD1, FOXF1, BDNF, Cdkl5, RPL11 and RPL5) [17, 20, 21]. FBXW7, a member of the F-box family of proteins, has been widely characterized as a tumor suppressor gene in many types of cancer. FBXW7 inhibits cancer cell survival, proliferation, cycle, differentiation, and metabolism; tumor metastasis; and drug resistance, and promotes apoptosis [42, 43]. FBXW7 expression is frequently downregulated in many human cancers, such as lung cancer, breast cancer, colorectal cancer, liver cancer, gastric cancer, pancreatic cancer, cervical cancer, prostate cancer, and esophageal cancer [44]. Loss-of-function mutations in FBXW7 are frequently found in human cancers, and the mutation rate across all cancers is approximately 6% [45]. Recent studies have shown that FBXW7 suppresses the proliferation, migration and invasion of cholangiocarcinoma, glioma, colorectal, breast and prostate cancer cells [46, 47]. The present study further demonstrated that FBXW7 is frequently downregulated in human GC tissues and that FBXW7 expression is correlated with the clinicopathologic features of GC. Overexpression of FBXW7 suppressed GC cell migration and invasion, while silencing FBXW7 promoted cell migration and invasion. Cotransfection with MECP2 siRNA and FBXW7 siRNA rescued the effects of MECP2 knockdown on cell migration and invasion. These findings suggest that MECP2 promotes GC cell migration and invasion by suppressing FBXW7 transcription by binding to the methylated CpG islands in the promoter region of FBXW7.

FBXW7 is a subunit of an SCF-type ubiquitin ligase complex that induces the ubiquitination and proteasomal degradation of oncoproteins, including SREBP1, Cyclin E, c-Jun, c-Myc, mTOR,

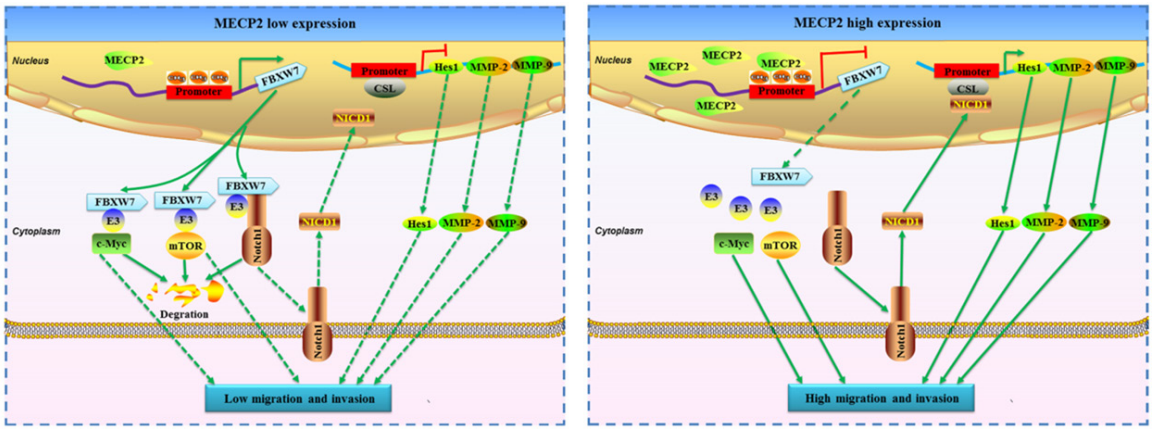

Figure 8. Proposed model for the effects of MECP2 on GC migration and invasion. MECP2 enhances GC cell migration and invasion by binding to the methylated CpG sites in the FBXW7 promoter region and repressing FBXW7 transcription, thereby promoting signaling through the Notch1/c-Myc/mTOR pathways.

Notch1, Notch4, MCL-1, KLF5 and MCL-1 [48-51]. This study showed that MECP2 increased the protein expression of c-Myc, mTOR, and Notch1 by inhibiting FBXW7 transcription and then preventing ubiquitination-mediated degradation of oncoproteins. C-Myc is a member of the Myc gene family that is involved in multiple biological processes, such as embryonic development, cell proliferation, cell cycle progression, apoptosis, differentiation, and protein synthesis [52], and is frequently amplified in many human cancers and promotes cell proliferation, migration and invasion [53]. MTOR acts as a serine/threonine protein kinase that modulates cell proliferation, cell motility, cell survival, protein synthesis, autophagy and cell cycle progression, and activation of the mTOR pathway promotes cancer cell proliferation, migration and invasion [54]. The Notch signaling pathways regulate cell differentiation, cell proliferation and apoptotic events [55]. Notch1-4 are transmembrane proteins that interact with ligands of the Delta-like and Jagged families. Binding of a ligand to its receptor leads to cleavage of the Notch receptor [56] and generation of the Notch1 intracellular domain (NICD1). NICD1 enters the nucleus and promotes Hes1, MMP-2 and MMP-9 expression in some cancers [57-59]. Previous studies have confirmed that Notch1 is upregulated in gastric cancer, liver cancer and ovarian cancer [60-62]. The present study revealed that by regulating the FBXW7/Notch1 signaling pathway, MECP2 upregulates Hes1, MMP-2 and MMP-9 expression. MECP2 promotes the migration and invasion of GC cells by regulating the Notch1/c-Myc/mTOR signaling pathways through inhibition of FBXW7 transcription (**Figure 8**).

Conclusions

In summary, this study demonstrates that MECP2 promotes GC cell migration and invasion through regulation of the Notch1/c-Myc/mTOR signaling pathways by repressing the transcription of FBXW7. MECP2 is upregulated and FBXW7 is downregulated in GC tissues, and their levels are closely correlated with clinicopathological features. These findings indicate that MECP2 may be a novel effective therapeutic target in GC.

Acknowledgements

This work was supported by the National Natural Science Foundation of China (81972603, 81772985, 81702918), the Natural Science Foundation of Shaanxi Province (2020JM-074, 2017JM8112), and Shaanxi Province Key Science and Technology Innovation Team (2020TD-039).

Disclosure of conflict of interest

None.

Address correspondence to: Dongdong Tong, Department of Cell Biology and Genetics, School of Basic Medical Sciences, Xi'an Jiaotong University Health Science Center, Xi'an 710061, Shaanxi, China. E-mail: tongdd@xjtu.edu.cn; Chen Huang, Department of Cell Biology and Genetics, School of

Basic Medical Sciences, Xi'an Jiaotong University Health Science Center, Xi'an 710061, Shaanxi, China. E-mail: hchen@xjtu.edu.cn

References

[1] Bray F, Ferlay J, Soerjomataram I, Siegel RL, Torre LA and Jemal A. Global cancer statistics 2018: GLOBOCAN estimates of incidence and mortality worldwide for 36 cancers in 185 countries. CA Cancer J Clin 2018; 68: 394-424.

[2] Siegel RL, Miller KD and Jemal A. Cancer statistics, 2016. CA Cancer J Clin 2016; 66: 7-30.

[3] Chen W, Zheng R, Baade PD, Zhang S, Zeng H, Bray F, Jemal A, Yu XQ and He J. Cancer statistics in China, 2015. CA Cancer J Clin 2016; 66: 115-132.

[4] Cancer Genome Atlas Research Network. Comprehensive molecular characterization of gastric adenocarcinoma. Nature 2014; 513: 202-209.

[5] Sun TT, He J, Liang Q, Ren LL, Yan TT, Yu TC, Tang JY, Bao YJ, Hu Y, Lin Y, Sun D, Chen YX, Hong J, Chen H, Zou W and Fang JY. LncRNA GClnc1 promotes gastric carcinogenesis and may act as a modular scaffold of WDR5 and KAT2A complexes to specify the histone modification pattern. Cancer Discov 2016; 6: 784-801.

[6] Zhang JX, He WL, Feng ZH, Chen DL, Gao Y, He Y, Qin K, Zheng ZS, Chen C, Weng HW, Yun M, Ye S, Xu RH and Xie D. A positive feedback loop consisting of C12orf59/NF-κB/CDH11 promotes gastric cancer invasion and metastasis. J Exp Clin Cancer Res 2019; 38: 164.

[7] Vieira JP, Lopes F, Silva-Fernandes A, Sousa MV, Moura S, Sousa S, Costa BM, Barbosa M, Ylstra B, Temudo T, Lourenço T and Maciel P. Variant Rett syndrome in a girl with a pericentric X-chromosome inversion leading to epigenetic changes and overexpression of the MECP2 gene. Int J Dev Neurosci 2015; 46: 82-87.

[8] Chahrour M, Jung SY, Shaw C, Zhou X, Wong ST, Qin J and Zoghbi HY. MeCP2, a key contributor to neurological disease, activates and represses transcription. Science 2008; 320: 1224-1229.

[9] Mellén M, Ayata P, Dewell S, Kriaucionis S and Heintz N. MeCP2 binds to 5hmC enriched within active genes and accessible chromatin in the nervous system. Cell 2012; 151: 1417-1430.

[10] Hite KC, Adams VH and Hansen JC. Recent advances in MeCP2 structure and function. Biochem Cell Biol 2009; 87: 219-227.

[11] Sinnett SE and Gray SJ. Recent endeavors in MECP2 gene transfer for gene therapy of Rett syndrome. Discov Med 2017; 24: 153-159.

[12] Gadalla KK, Bailey ME and Cobb SR. MeCP2 and Rett syndrome: reversibility and potential avenues for therapy. Biochem J 2011; 439: 1-14.

[13] Carouge D, Host L, Aunis D, Zwiller J and Anglard P. CDKL5 is a brain MeCP2 target gene regulated by DNA methylation. Neurobiol Dis 2010; 2010: 414-424.

[14] McGraw CM, Samaco RC and Zoghbi HY. Adult neural function requires MeCP2. Science 2011; 333: 186.

[15] Baker SA, Chen L, Wilkins AD, Yu P, Lichtarge O and Zoghbi HY. An AT-hook domain in MeCP2 determines the clinical course of Rett syndrome and related disorders. Cell 2013; 152: 984-996.

[16] Shin J, Ming GL and Song H. By hook or by crook: multifaceted DNA-binding properties of MeCP2. Cell 2013; 152: 940-942.

[17] Gabel HW, Kinde B, Stroud H, Gilbert CS, Harmin DA, Kastan NR, Hemberg M, Ebert DH and Greenberg ME. Disruption of DNA-methylation-dependent long gene repression in Rett syndrome. Nature 2015; 522: 89-93.

[18] Neupane M, Clark AP, Landini S, Birkbak NJ, Eklund AC, Lim E, Culhane AC, Barry WT, Schumacher SE, Beroukhim R, Szallasi Z, Vidal M, Hill DE and Silver DP. MECP2 is a frequently amplified oncogene with a novel epigenetic mechanism that mimics the role of activated RAS in malignancy. Cancer Discov 2016; 6: 45-58.

[19] Zhao LY, Zhang J, Guo B, Yang J, Han J, Zhao XG, Wang XF, Liu LY, Li ZF, Song TS and Huang C. MECP2 promotes cell proliferation by activating ERK1/2 and inhibiting p38 activity in human hepatocellular carcinoma HEPG2 cells. Cell Mol Biol (Noisy-le-Grand) 2013; Suppl 59: OL1876-1881.

[20] Tong D, Zhang J, Wang X, Li Q, Liu LY, Yang J, Guo B, Ni L, Zhao L and Huang C. MeCP2 facilitates breast cancer growth via promoting ubiquitination-mediated P53 degradation by inhibiting RPL5/RPL11 transcription. Oncogenesis 2020; 9: 56.

[21] Zhao L, Liu Y, Tong D, Qin Y, Yang J, Xue M, Du N, Liu L, Guo B, Hou N, Han J, Liu S, Liu N, Zhao X, Wang L, Chen Y and Huang C. MeCP2 promotes gastric cancer progression through regulating FOXF1/Wnt5a/beta-catenin and MYOD1/Caspase-3 signaling pathways. EbioMedicine 2017; 16: 87-100.

[22] Zhao LY, Tong DD, Xue M, Ma HL, Liu SY, Yang J, Liu YX, Guo B, Ni L, Liu LY, Qin YN, Wang LM, Zhao XG and Huang C. MeCP2, a target of miR-638, facilitates gastric cancer cell proliferation through activation of the MEK1/2-ERK1/2 signaling pathway by upregulating GIT1. Oncogenesis 2017; 6: e368.

[23] Kasowski M, Grubert F, Heffelfinger C, Hariharan M, Asabere A, Waszak SM, Habegger L, Rozowsky J, Shi M, Urban AE, Hong MY, Karczewski KJ, Huber W, Weissman SM, Gerstein MB, Korbel JO and Snyder M. Variation in transcription factor binding among humans. Science 2010; 328: 232-235.

[24] Qian Z, Zhu G, Tang L, Wang M, Zhang L, Fu J, Huang C, Fan S, Sun Y, Lv J, Dong H, Gao B, Su X, Yu D, Zang J, Zhang X, Ji J and Ji Q. Whole genome gene copy number profiling of gastric cancer identifies PAK1 and KRAS gene amplification as therapy targets. Genes Chromosomes Cancer 2014; 53: 883-894.

[25] Eftang LL, Esbensen Y, Tannæs TM, Blomm GP, Bukholm IR and Bukholm G. Up-regulation of CLDN1 in gastric cancer is correlated with reduced survival. BMC Cancer 2013; 13: 586.

[26] Cheng Y and Li G. Role of the ubiquitin ligase Fbw7 in cancer progression. Cancer Metastasis Rev 2012; 31: 75-87.

[27] Mao JH, Kim IJ, Wu D, Climent J, Kang HC, DelRosario R and Balmain A. FBXW7 targets mTOR for degradation and cooperates with PTEN in tumor suppression. Science 2008; 321: 1499-1502.

[28] Welcker M and Clurman BE. FBW7 ubiquitin ligase: a tumour suppressor at the crossroads of cell division, growth and differentiation. Nat Rev Cancer 2008; 8: 83-93.

[29] Chaturvedi R, de Sablet T, Asim M, Piazuelo MB, Barry DP, Verriere TG, Sierra JC, Hardbower DM, Delgado AG, Schneider BG, Israel DA, Romero-Gallo J, Nagy TA, Morgan DR, Murray-Stewart T, Bravo LE, Peek RM Jr, Fox JG, Woster PM, Casero RA Jr, Correa P and Wilson KT. Increased Helicobacter pylori-associated gastric cancer risk in the Andean region of Colombia is mediated byspermine oxidase. Oncogene 2015; 34: 3429-3440.

[30] Müller HM, Fiegl H, Goebel G, Hubalek MM, Widschwendter A, Müller-Holzner E, Marth C and Widschwendter M. MeCP2 and MBD2 expression in human neoplastic and non-neoplastic breast tissue and its association with oestrogen receptor status. Br J Cancer 2003; 89: 1934-1939.

[31] Meng G, Lv Y, Dai H, Zhang X and Guo QN. Epigenetic silencing of methyl-CpG-binding protein 2 gene affects proliferation, invasion, migration, and apoptosis of human osteosarcoma cells. Tumour Biol 2014; 35: 11819-11827.

[32] Murphy DM, Buckley PG, Das S, Watters KM, Bryan K and Stallings RL. Colocalization of the oncogenic transcription factor MYCN and the DNA methyl binding proteinMeCP2 at genomic sites in neuroblastoma. PLoS One 2011; 6: e21436.

[33] Babbio F, Castiglioni I, Cassina C, Gariboldi MB, Pistore C, Magnani E, Badaracco G, Monti E and Bonapace IM. Knock-down of methyl CpG-binding protein 2 (MeCP2) causes alterations in cell proliferation and nuclear lamins expression in mammalian cells. BMC Cell Biol 2012; 11: 13-19.

[34] Sharma K, Singh J, Frost EE and Pillai PP. MeCP2 overexpression inhibits proliferation, migration and invasion of C6 glioma by modulating ERK signaling and gene expression. Neurosci Lett 2018; 674: 42-48.

[35] Liu Y, Jin X, Li Y, Ruan Y, Lu Y, Yang M, Lin D, Song P, Guo Y, Zhao S, Dong B, Xie YP, Dang Q and Quan C. DNA methylation of claudin-6 promotes breast cancer cell migration and invasion by recruiting MeCP2 and deacetylating H3Ac and H4Ac. J Exp Clin Cancer Res 2016; 35: 120.

[36] Itoh Y and Nagase H. Matrix metalloproteinases in cancer. Essays Biochem 2002; 38: 21-36.

[37] Nagase H, Visse R and Murphy G. Structure and function of matrix metalloproteinases and TIMPs. Cardiovasc Res 2006; 69: 562-573.

[38] Komatsu K, Nakanishi Y, Nemoto N, Hori T, Sawada T and Kobayashi M. Expression and quantitative analysis of matrix metalloproteinase-2 and -9 in human gliomas. Brain Tumor Pathol 2004; 21: 105-112.

[39] Köhrmann A, Kammerer U, Kapp M, Dietl J and Anacker J. Expression of matrix metalloproteinases (MMPs) in primary human breast cancer and breast cancer cell lines: new findings and review of the literature. BMC Cancer 2009; 9: 188.

[40] Lu S, Zhang Z, Chen M, Li C, Liu L and Li Y. Silibinin inhibits the migration and invasion of human gastric cancer SGC7901 cells by downregulating MMP-2 and MMP-9 expression via the p38MAPK signaling pathway. Oncol Lett 2017; 14: 7577-7582.

[41] Pagliara V, Nasso R, Di Donato P, Finore I, Poli A, Masullo M and Arcone R. Lemon peel polyphenol extract reduces interleukin-6-induced cell migration, invasiveness, and matrix metalloproteinase-9/2 expression in human gastric adenocarcinoma MKN-28 and AGS cell lines. Biomolecules 2019; 9: 833.

[42] Zhan P, Wang Y, Zhao S, Liu C, Wang Y, Wen M, Mao JH, Wei G and Zhang P. FBXW7 negatively regulates ENO1 expression and function in colorectal cancer. Lab Invest 2015; 95: 995-1004.

[43] Wang Z, Inuzuka H, Zhong J, Wan L, Fukushima H, Sarkar FH and Wei W. Tumor suppressor functions of FBW7 in cancer development and progression. FEBS Lett 2012; 586: 1409-1418.

[44] Yeh CH, Bellon M and Nicot C. FBXW7: a critical tumor suppressor of human cancers. Mol Cancer 2018; 17: 115.
[45] Akhoondi S, Sun D, von der Lehr N, Apostolidou S, Klotz K, Maljukova A, Cepeda D, Fiegl H, Dafou D, Marth C, Mueller-Holzner E, Corcoran M, Dagnell M, Nejad SZ, Nayer BN, Zali MR, Hansson J, Egyhazi S, Petersson F, Sangfelt P, Nordgren H, Grander D, Reed SI, Widschwendter M, Sangfelt O and Spruck C. FBXW7/hCDC4 is a general tumor suppressor in human cancer. Cancer Res 2007; 67: 9006-9012.
[46] Yang H, Lu X, Liu Z, Chen L, Xu Y, Wang Y, Wei G and Chen Y. FBXW7 suppresses epithelial-mesenchymal transition, stemness and metastatic potential of cholangiocarcinoma cells. Oncotarget 2015; 6: 6310-6325.
[47] Wang Y, Liu Y, Lu J, Zhang P, Wang Y, Xu Y, Wang Z, Mao JH and Wei G. Rapamycin inhibits FBXW7 loss-induced epithelial-mesenchymal transition and cancer stem cell-like characteristics in colorectal cancer cells. Biochem Biophys Res Commun 2013; 434: 352-356.
[48] Xiao G, Li Y, Wang M, Li X, Qin S, Sun X, Liang R, Zhang B, Du N, Xu C, Ren H and Liu D. FBXW7 suppresses epithelial-mesenchymal transition and chemo-resistance of non-small-cell lung cancer cells by targeting snai1 for ubiquitin-dependent degradation. Cell Prolif 2018; 51: e12473.
[49] Jin X, Yang C, Fan P, Xiao J, Zhang W, Zhan S, Liu T, Wang D and Wu H. CDK5/FBW7-dependent ubiquitination and degradation of EZH2 inhibits pancreatic cancer cell migration and invasion. J Biol Chem 2017; 292: 6269-6280.
[50] Tu K, Zheng X, Yin G, Zan X, Yao Y and Liu Q. Evaluation of Fbxw7 expression and its correlation with expression of SREBP-1 in a mouse model of NAFLD. Mol Med Rep 2012; 6: 525-530.
[51] Inuzuka H, Shaik S, Onoyama I, Gao D, Tseng A, Maser RS, Zhai B, Wan L, Gutierrez A, Lau AW, Xiao Y, Christie AL, Aster J, Settleman J, Gygi SP, Kung AL, Look T, Nakayama KI, DePinho RA and Wei W. SCF(FBW7) regulates cellular apoptosis by targeting MCL1 for ubiquitylation and destruction. Nature 2011; 471: 104-109.
[52] Chen BJ, Wu YL, Tanaka Y and Zhang W. Small molecules targeting c-Myc oncogene: promising anti-cancer therapeutics. Int J Biol Sci 2014; 10: 1084-1096.
[53] Dang CV. MYC on the path to cancer. Cell 2012; 149: 22-35.
[54] Hay N and Sonenberg N. Upstream and downstream of mTOR. Genes Dev 2004; 218: 1926-1945.
[55] Artavanis-Tsakonas S, Rand MD and Lake RJ. Notch signaling: cell fate control and signal integration in development. Science 1999; 284: 770-776.
[56] Bedogni B, Warneke JA, Nickoloff BJ, Giaccia AJ and Powell MB. Notch1 is an effector of Akt and hypoxia in melanoma development. J Clin Invest 2008; 118: 3660-3670.
[57] Minella AC and Clurman BE. Mechanisms of tumor suppression by the SCF (Fbw7). Cell Cycle 2005; 4: 1356-1359.
[58] Wang X, Zhang J, Zhou L, Sun W, Zheng ZG, Lu P, Gao Y, Yang XS, Zhang ZC, Tao KS and Dou KF. Fbxw7 regulates hepatocellular carcinoma migration and invasion via Notch1 signaling pathway. Int J Oncol 2015; 47: 231-243.
[59] Yu B, Wei J, Qian X, Lei D, Ma Q and Liu Y. Notch1 signaling pathway participates in cancer invasion byregulating MMPs in lingual squamous cell carcinoma. Oncol Rep 2012; 27: 547-552.
[60] Sun L, Hui AM, Su Q, Vortmeyer A, Kotliarov Y, Pastorino S, Passaniti A, Menon J, Walling J, Bailey R, Rosenblum M, Mikkelsen T and Fine HA. Neuronal and glioma-derived stem cell factor induces angiogenesis within the brain. Cancer Cell 2006; 9: 287-300.
[61] D'Errico M, de Rinaldis E, Blasi MF, Viti V, Falchetti M, Calcagnile A, Sera F, Saieva C, Ottini L, Palli D, Palombo F, Giuliani A and Dogliotti E. Genomewide expression profile of sporadic gastric cancers with microsatellite instability. Eur J Cancer 2009; 45: 461-469.
[62] Zhou L, Zhang N, Song W, You N, Li Q, Sun W, Zhang Y, Wang D and Dou K. The significance of Notch1 compared with Notch3 in high metastasis and poor overall survival in hepatocellular carcinoma. PLoS One 2013; 8: e57382.

Supplementary Table 1. Primer sequences used for qRT-PCR in this study

Gene	Sequence
MECP2-F	5'-GCCGAGAGCTATGGACAGCA-3'
MECP2-R	5'-CCAACCTCAGACAGGTTTCCAG-3'
FBXW7-F	5'-AAAGAGTTGTTAGCGGTTCTCG-3'
FBXW7-R	5'-CCACATGGATACCATCAAACTG-3'
c-Myc-F	5'-TCGGACTCTCTGCTCTCCTC-3'
c-Myc-R	5'-CTGCATAATTGTGCTGGTGC-3'
mTOR-F	5'-CTGGGACTCAAATGTGTGCAGTTC-3'
mTOR-R	5'-GAACAATAGGGTGAATGATCCGGG-3'
Notch1-F	5'-ATCGACATGGCCGAATGGAA-3'
Notch1-R	5'-ATGATGTCCACGCCCTTCTG-3'
Hes1-F	5'-AACCAAAGACAGCATCTGAGCAC-3'
Hes1-R	5'-TGTAGACCATGTAGTTGAGGTCA-3'
MMP-2-F	5'-AAGTCTGAAGAGCGTGAAGTTTGGA-3'
MMP-2-R	5'-TGAGGGTTGGTGGGATTGGAG-3'
MMP-9-F	5'-AGTCCACCCTTGTGCTCTTCCC-3'
MMP-9-R	5'-TCTGCCACCCGAGTGTAACCAT-3'
β-Actin-F	5'-TGGCACC CAGCACAATGAA-3'
β-Actin-R	5'-CTAAGTCATAGTCCGCCTAGAAGCA-3'

Supplementary Table 2. Sequences of MECP2 MT recombinant plasmids

Name	Sequence
MECP2-WT MBD sequence	5'-AGGGGCCCTATGTATGATGACCCTACACTGCCCGAGGGCTGGACCAGGAAACT-GAAGCAGAGGAAGTCCGGAAGGAGCGCCGGCAAATACGATGTCTACCTGATTA-ACCCCCAGGGCAAGGCCTTTAGATCCAAGGTGGAGCTGATCGCCTACTTTGAGAAGGTCG-GCGACACATCCCTAGACCCGAATGACTTCGACTTCACAGTGACCGGCAGAGGA-3'
MECP2-MT1 MBD sequence	5'-AGGGGCCCTATGTATGATGACCCTACACTGCCCGAGGGCTGGACCAGGAAACT-GAAGCAGAGGAAGTCCGGAGATCAGTATCACGAAGGTCGCGTCTACCTGATTA-ACCCCCAGGGCAAGGCCTTTAGATCCAAGGTGGAGCTGATCGCCTACTTTGAGAAGGTCG-GCGACACATCCCTAGACCCGAATGACTTCGACTTCACAGTGACCGGCAGAGGA-3'
MECP2-MT2 MBD sequence	5'-AGGGGCCCTATGTATGATGACCCTACACTGCCCGAGGGCTGGACCAGGAAACT-GAAGCAGAGGAAGTCCGGAAGGAGCGCCGGCAAATACGATGTCTACCTGATTA-ACCCCCAGGGCAAGGCCTTTAGATCCAAGGTGGAGCTGCATGACAAGCAGGCCGAGAGTG-GCGACACATCCCTAGACCCGAATGACTTCGACTTCACAGTGACCGGCAGAGGA-3'

Green: Wild type DNA sequence of MBD region. Red: Mutation type DNA sequence of MBD region.

Supplementary Table 3. Sequences of siRNA

Name	Sequence
negative siRNA (NC-siRNA) sense	5'-UUCUCCGAACGUGUCACGUTT-3'
negative siRNA (NC-siRNA) antisense	5'-ACGUGACACGUUCGGAGAATT-3'
si-MeCP2-1 sense	5'-GCUUAAGCAAAGGAAAUCUTT-3'
si-MeCP2-1 antisense	5'-AGAUUUCCUUUGCUUAAGCTT-3'
si-MeCP2-2 sense	5'-GCUUCCCGAUUAACUGAAATT-3'
si-MeCP2-2 antisense	5'-UUUCAGUUAAUCGGGAAGCTT-3'
si-FBXW7-1 sense	5'-GCACAGAAUUGAUACUAACTT-3'
si-FBXW7-1 antisense	5'-GUUAGUAUCAAUUCUGUGCTG-3'
si-FBXW7-2 sense	5'-CCUUAUAUGGGCAUACUUCTT-3'
si-FBXW7-2 antisense	5'-GAAGUAUGCCCAUAUAAGGTG-3'

Supplementary Table 4. Information on antibodies used for the correlation analysis

Antibody	WB	IHC	Specificity	Company
MECP2 (sc-20700)	1:1000	1:100	Rabbit polyclonal	Santa Cruz Biotechnology
FBXW7 (ab227677)	1:1000	1:100	Rabbit Monoclonal	Abcam
mTOR (sc-517464)	1:1000	-	Mouse monoclonal	Santa Cruz Biotechnology
Notch1 (ab65297)	1:1000	-	Rabbit polyclonal	Abcam
Hes1 (ab71599)	1:1000	-	Rabbit polyclonal	Abcam
MMP-2 (sc-13594)	1:1000	-	Mouse monoclonal	Santa Cruz Biotechnology
MMP-9 (sc-393859)	1:1000	-	Mouse monoclonal	Santa Cruz Biotechnology
NICD1 (ab52301)	1:1000	-	Rabbit polyclonal	Abcam
c-Myc (13987)	1:1000	-	Rabbit Monoclonal	Cell Signaling Technology
Lamin A (sc-518013)	1:1000	-	Rabbit Monoclonal	Cell Signaling Technology
β-Actin (sc-8432)	1:3000	-	Mouse Monoclonal	Santa Cruz Biotechnology
MECP2 ChIP Grade (ab2828)	-	-	Rabbit polyclonal	Abcam
GFP ChIP Grade (ab290)	-	-	Rabbit polyclonal	Abcam
IgG ChIP Grade (ab171870)	-	-	Rabbit polyclonal	Abcam

Supplementary Table 5. Sequences of recombinant plasmids

Name	Sequence
Negative control	5'-AAAAGAGGCTTGCACAGTGCATTCAAGACGTGCACTGTGCAAGCCTCTTTT-3'
MeCP2 shRNA	5'-TGCTTAAGCAAAGGAAATCTCTCGAGAGATTTCCTTTGCTTAAGCTTTTTTC-3'

Supplementary Table 6. Patient characteristics and clinicopathologic correlation of MECP2 expression in GC

Characteristics	Number of cases	MECP2 mRNA expression		*P-value*
		High (n = 127)	Low (n = 39)	
Age				0.879
≥ 60 years	75	59	16	
< 60 years	91	68	23	
Sex				0.802
Male	102	77	25	
Female	64	50	14	
Histology				0.023*
Well	86	59	27	
Moderate	32	24	8	
poor	48	44	4	
Size				0.0016*
< 50 mm	77	51	26	
≥ 50 mm	89	76	13	
Lymph node metastasis				0.0002*
Absent	58	53	5	
Present	108	74	34	
Lymphatic invasion				0.0052*
Absent	54	47	7	
Present	112	80	32	
Venous invasion				0.056
Absent	93	74	19	
Present	73	53	20	

Serosal invasion				0.008*
Absent	57	49	8	
Present	109	78	31	
Liver metastasis				0.109
Absent	124	97	27	
Present	42	30	12	
T Stage				0.0037*
T1	55	34	21	
T2	42	34	8	
T3	39	32	7	
T4	30	27	3	

*P < 0.05.

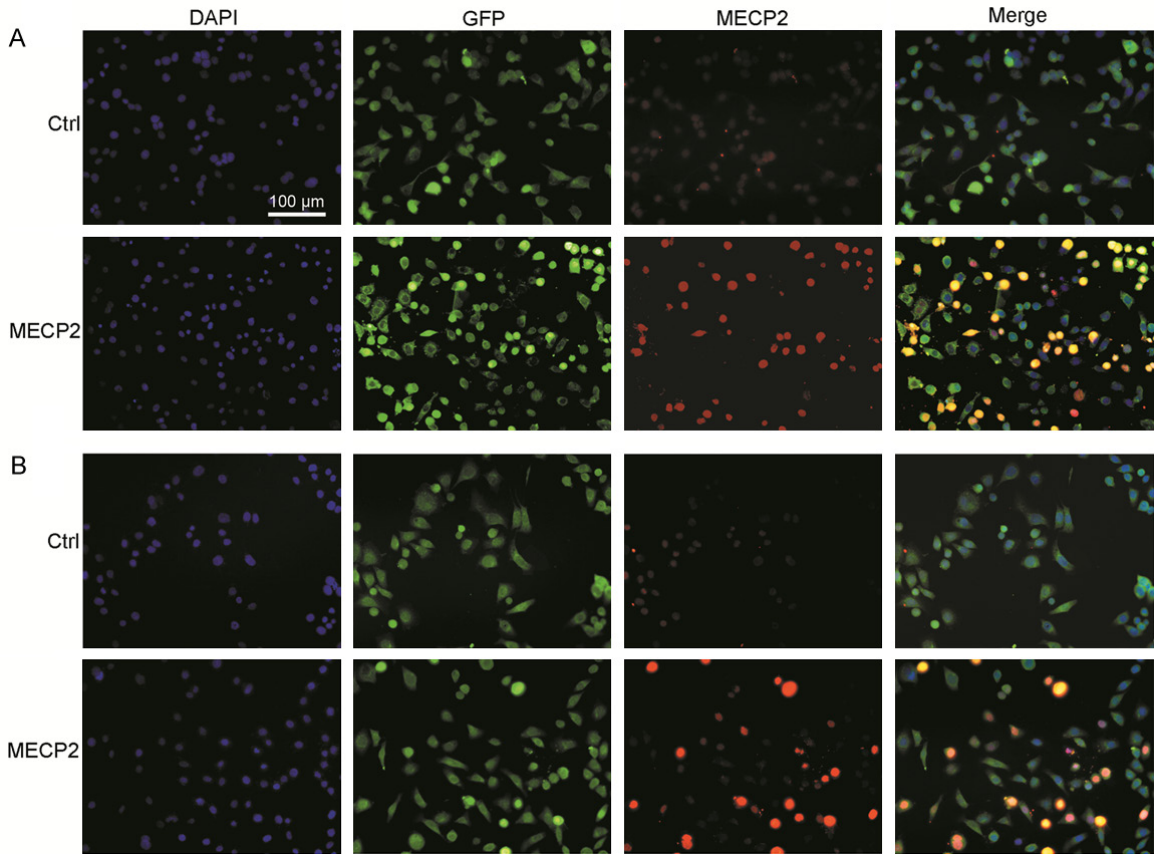

Supplementary Figure 1. The exogenous level of MECP2 enhances after transfection with the MECP2 overexpression plasmid. A. The exogenous level of MECP2 after transfection in BGC-823 cells. B. The exogenous level of MECP2 after transfection in MKN-45 cells. n = 3.

Supplementary Table 7. Sequences of MECP2 binding to FBXW7 promoter region

Gene	Sequence
FBXW7	GAATCAGAGTCACGTATTCTGTTTTTCACTAAGATATTGCAAAGAGAAATGTAGTC ATTTTCTAAAATACTGTACCCAAAATACAGTAGAAGCTGTATTTTGGGAAGGAGGG GAGGACAAACTAAGAAACAAACTATAGTTTGAATGTAGGTTGCACTCTGTCAAAG TTGCTTACTAACTTTAGGACCTACTTTTATTGCTTATGGATTGGTTAAAAATTACGGT ATTTTTTTTTTTTTTGAGACAGAGTCTTGCTCTGTCACCCAGGCTGGAGTGCAATGG AGCGATCTTGGCTCACTGCAACCTCCGCCTCCCAGGTTCAAGCGATTCTCATGCCT CAGCCTCCCAAATAGCTGGGACTACAGGCATGTGCTACCACGCCTGGCTAATTTTT TTTGTATTTTTAGTAGAGATGGGGTTTCACCATGTGGGTCAGGCTGGTCTAGAACTC CTGACCTCAAAT

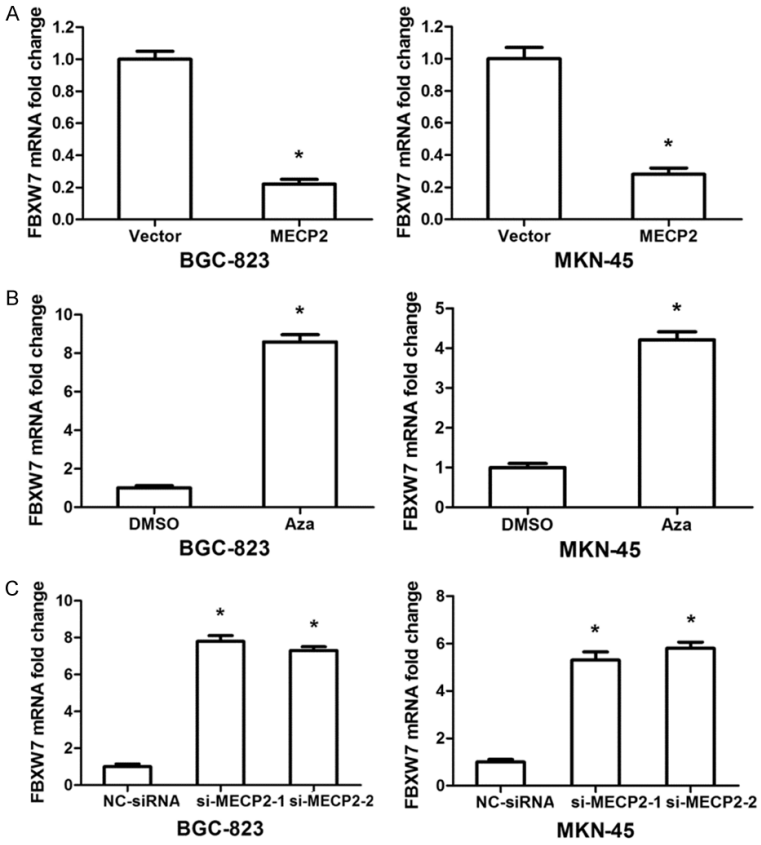

Supplementary Figure 2. MECP2 regulates FBXW7 mRNA expression in BGC-823 and MKN-45 cells. A. FBXW7 mRNA expression after transfection with the MECP2 overexpression plasmid. B. FBXW7 mRNA expression after transfection with methylation inhibitor Aza. C. FBXW7 mRNA expression after transfection with si-MECP2-1 and si-MECP2-2. n = 3, *P < 0.001.

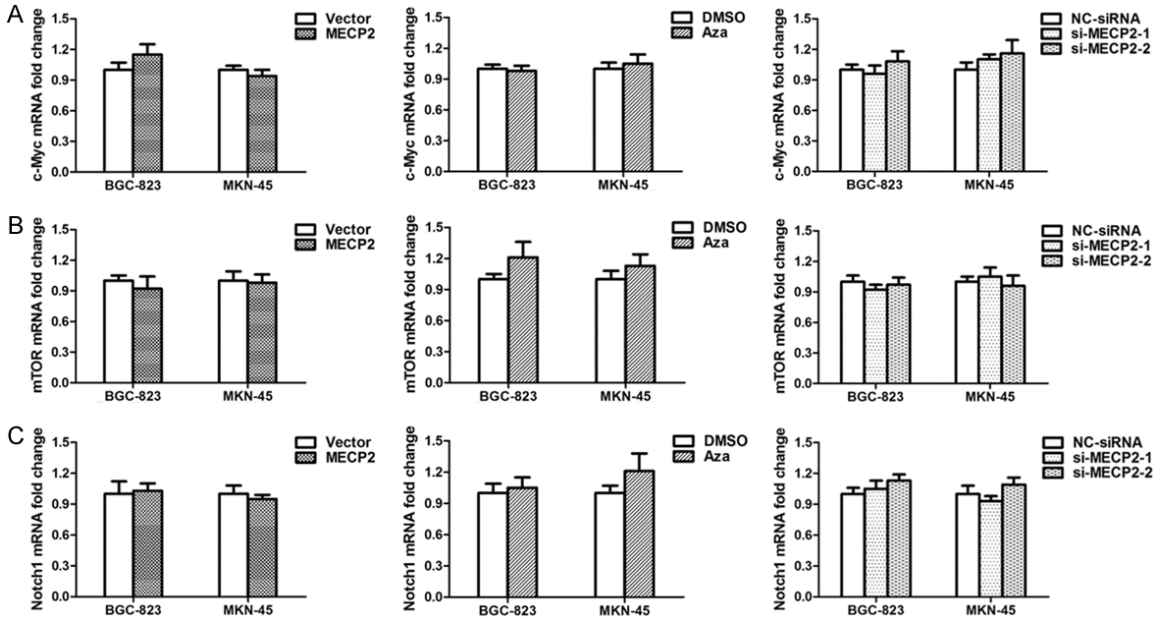

Supplementary Figure 3. MECP2 doesn't affect the mRNA expressions of Notch1, c-Myc and mTOR. A. C-Myc mRNA was detected in GC BGC-823 and MKN-45 cells after treatment with the MECP2 overexpression plasmid, methylation inhibitor Aza, MECP2-1 and si-MECP2-2. B. MTOR mRNA was determined in GC cells after treatment. C. Notch1 mRNA was measured in GC cells after treatment. n = 3.

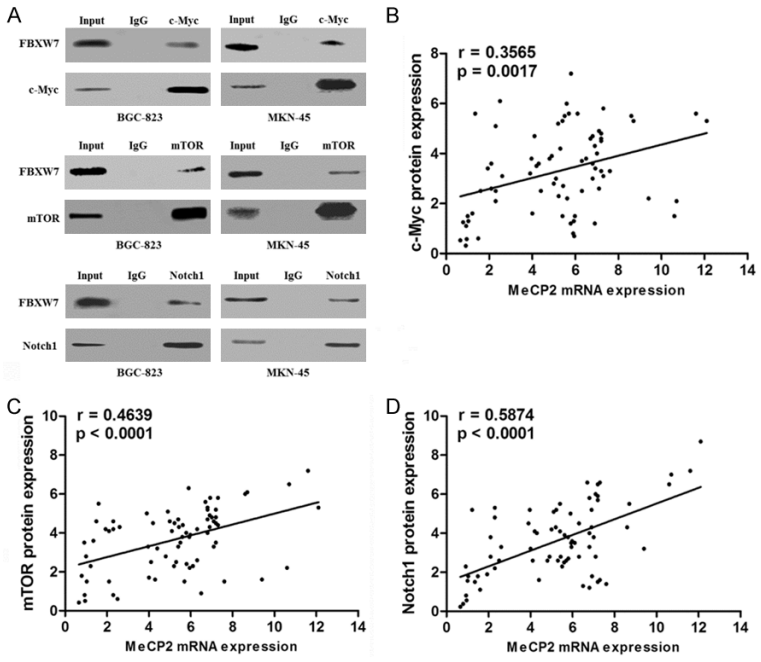

Supplementary Figure 4. MECP2 regulates the FBXW7-Notch1/c-Myc/mTOR signaling pathways. A. Co-IP experiments in BGC-823 and MKN-45 cells were performed using anti- c-MYC, anti-mTOR or anti-Notch1 antibodies, respectively. IgG was used as a control. B. MECP2 mRNA level is associated with the protein expression of c-MYC in human GC samples. C. MECP2 mRNA level is associated with the protein expression of mTOR. D. MECP2 mRNA level is associated with the protein expression of Notch1. n = 75.

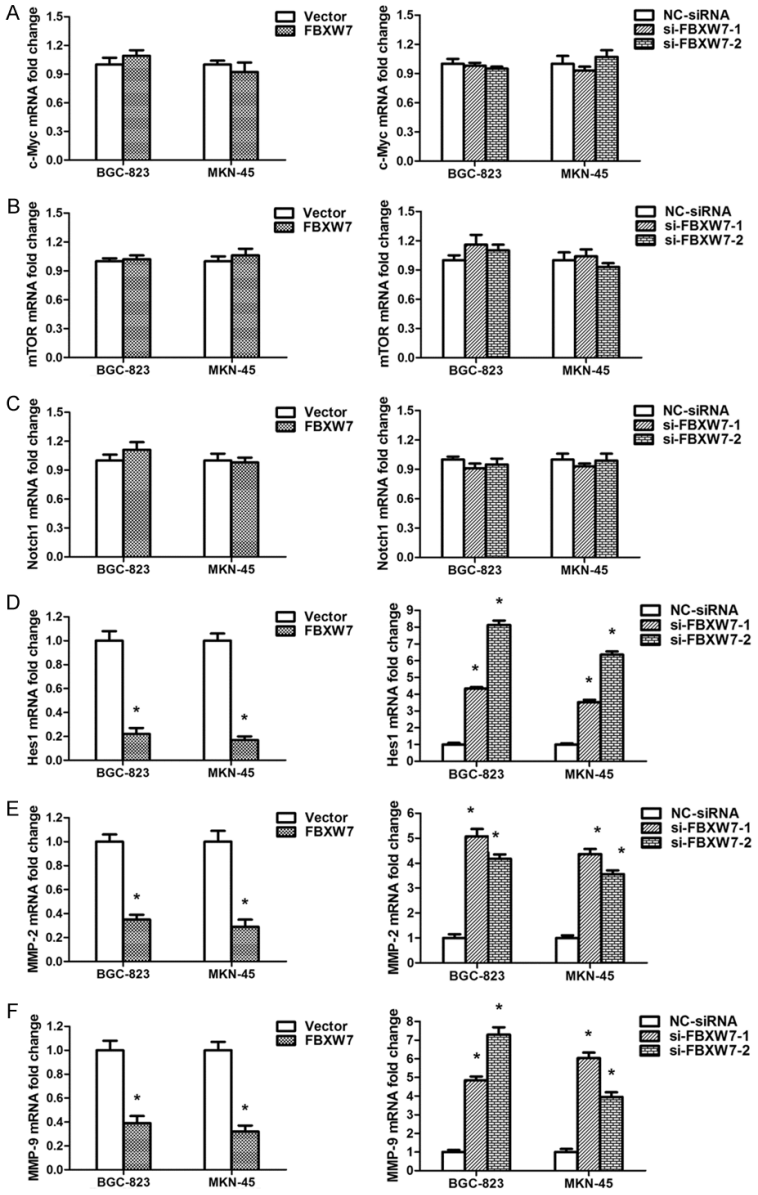

Supplementary Figure 5. FBXW7 regulates the mRNA expressions of c-Myc, mTOR, Notch1, Hes1, MMP-2 and MMP-9. A. C-Myc mRNA was determined in GC BGC-823 and MKN-45 cells after transfection with the FBXW7 overexpression plasmid, si-FBXW7-1 and si-FBXW7-2. B. MTOR mRNA was measured in GC cells after transfection. C. Notch1 mRNA was examined in GC cells after transfection. D. Hes1 mRNA was measured in GC cells after transfection. E. MMP-2 mRNA was examined in GC cells after transfection. F. MMP-9 mRNA was detected in GC cells after transfection. n = 3, *P < 0.001.

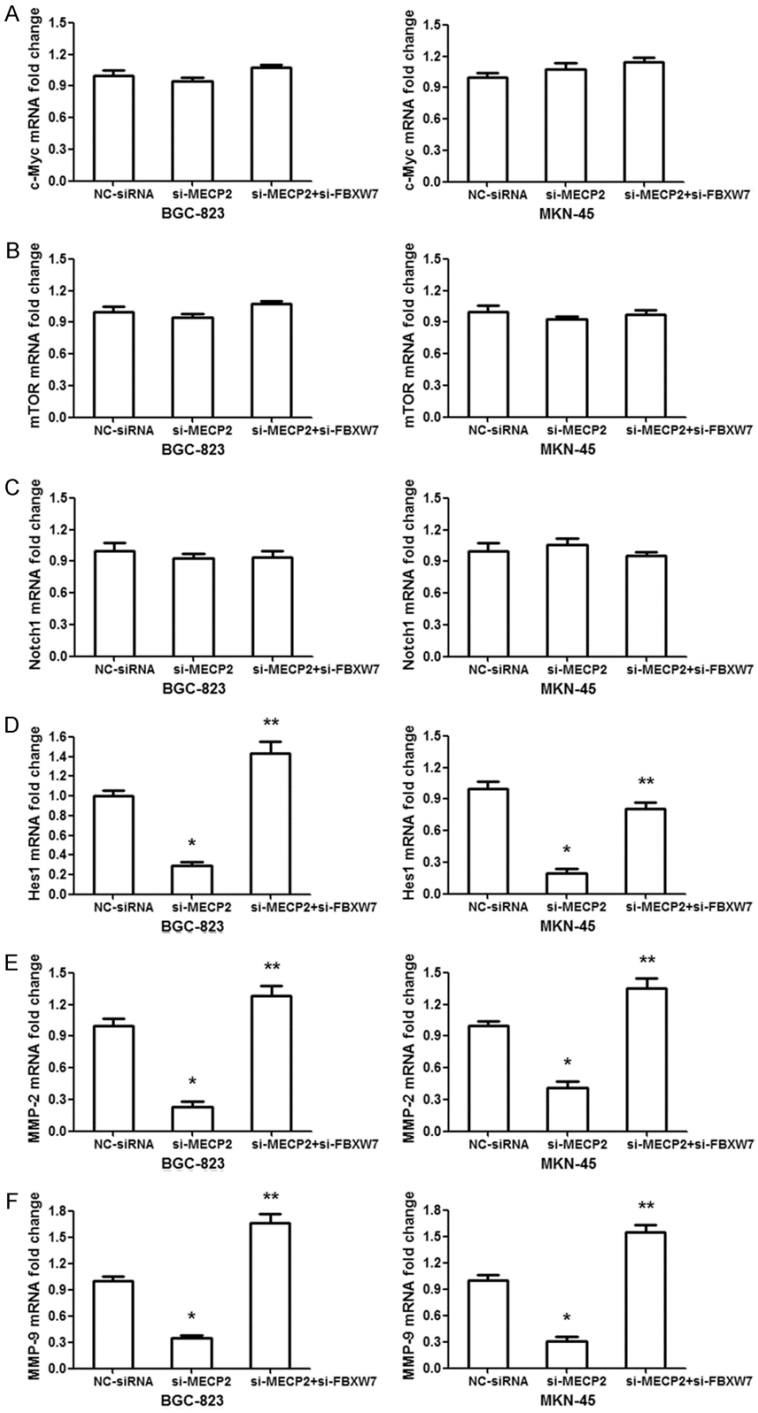

Supplementary Figure 6. Si-MECP2 and si-MECP2 + si-FBXW7 affect the mRNA expressions of c-Myc, mTOR, Notch1, Hes1, MMP-2 and MMP-9. A. C-Myc mRNA was measured in BGC-823 and MKN-45 cells after transfection with si-MECP2 alone or cotransfection with si-MECP2 and si-FBXW7. B. MTOR mRNA was examined in GC cells after transfection. C. Notch1 mRNA was detected in GC cells after transfection. D. Hes1 mRNA was examined in GC cells after transfection. E. MMP-2 mRNA was measured in GC cells after transfection. F. MMP-9 mRNA was detected in GC cells after transfection. n = 3, *P < 0.01, compared with NC-siRNA-transfected cells; **P < 0.01, compared with si-MECP2-transfected cells.